

The dynamics of high autoionizing Rydberg states of Ar

M. Bixon and Joshua Jortner

School of Chemistry, Tel Aviv University, 69978 Tel Aviv, Israel

(Received 12 April 1995; accepted 26 May 1995)

In this paper we present a theoretical study of the autoionization dynamics of high $^2P_{1/2}np'[3/2]_1$ Rydbergs (with the principal quantum numbers $n=100-280$) of Ar in weak homogeneous electric fields ($F=0.01-1.0$ V/cm), which were experimentally interrogated by time-resolved zero-electron kinetic energy (ZEKE) spectroscopy [M. Mühlfordt and U. Even, *J. Chem. Phys.* **103**, 4427 (1995)], and which exhibit a marked dilution (i.e., ~ 2 orders of magnitude lengthening) of the lifetimes relative to those inferred on the basis of the n^3 scaling law for the spectral linewidths of the np' ($n=12-24$) Rydbergs. The multichannel effective Hamiltonian (\mathbf{H}_{eff}) with several doorway state(s) (for excitation and decay) and pure escape states (for decay) was advanced and utilized to treat the dynamics of the mixed Stark manifold of the ZEKE Rydbergs. \mathbf{H}_{eff} of dimension $2n-1$ is then constructed for a n Rydberg manifold using independent experimental information on the (l dependent) quantum defects $\delta(l)$ and the (l, K, J dependent) decay widths, which are of the form $\Gamma_0(IKJ)/(n-\delta(l))^3$, with $\Gamma_0(IKJ)$ being the decay widths constants. Here, $l, K,$ and J are the azimuthal, the electronic and the total electronic angular momentum quantum numbers, respectively. Two coupling ranges are distinguished according to the strength of the reduced electric field $\bar{F}(n,p')=(F/\text{V cm}^{-1})n^5/3.4\times 10^9[\delta(p')(\text{mod}1)]$. Range (A); The onset of the effective coupling of the doorway and escape states, i.e., $0.7\leq\bar{F}(n,p')\leq 2$. Range (B); The strong mixing domain $\bar{F}(n,p')\geq 3$. The lifetimes in range (B) can be well represented by a nearly democratic mixing of all the doorway and escape states (IKJ), with the average value

$$\langle\tau(n)\rangle\approx\langle\tau_{\text{SM}}(n)\rangle=2n^4\hbar\left/\left[\sum_{(IJK)}\Gamma_0(IJK)\right]\right.$$

In range (B) $\langle\tau(n)\rangle$ increases with increasing n and is only weakly F dependent. Range (A) is characterized by a hierarchy of two time scales for the decay, with a short decay component, which manifests the residue of the doorway state, and a distribution of very long lifetimes with an average value $\langle\tau_{\text{LONG}}(n)\rangle\approx\eta(n)\langle\tau_{\text{SM}}(n)\rangle$, where $\eta(n)\approx 2-5$. In range (A), $\langle\tau_{\text{LONG}}(n)\rangle$ decreases with increasing n and decreases with increasing F , manifesting the enhancement of mixing. We identified range (B) for $n=150-280$, where a semiquantitative agreement between the experimental ZEKE lifetimes and spectra and our theory was obtained. A tentative identification of range (A) for lower n ($=100-150$) values was accomplished. We have also performed a theoretical study of the Ar autoionization dynamics via the $^2P_{1/2}nd'[3/2]_1$ doorway state, which was experimentally studied by Merkt [*J. Chem. Phys.* **100**, 2623 (1994)]. The onset of range (A) was identified in the region $n=70-80$, with the estimated lifetimes near the onset being in agreement with experiment. Our analysis explains the higher n onset for the np' doorway state mixing ($n\approx 100$ and $F\approx 0.1$ V/cm) than for the np' doorway state mixing ($n'=70-80$ for $F\approx 0.1$ V/cm). Experimental values of $\langle\tau_{\text{LONG}}(n)\rangle$ (around $n\approx 90$) in range (A), excited via the $^2P_{1/2}nd'[3/2]_1$ doorway state, are considerably longer than those predicted by our theory for l mixing. The discrepancy may be due to (lm_l) mixing, which presumably originates from Rydberg-ion collisions. © 1995 American Institute of Physics.

I. INTRODUCTION

High Rydberg states (characterized by principal quantum numbers $n=50-300$) of atoms, molecules, and clusters constitute one-electron excitations with a mean radius $\langle r\rangle=(3/2)n^2a_0$ (where a_0 is the Bohr radius), e.g., $\langle r\rangle\approx 1.0\mu$ for $n=112$. Such microsystems are of considerable interest in the context of the determination of fundamental physical constants,¹ the manifestation of long-range Casimir retardation forces, which are revealed on the distance scale of $r>137a_0$,² the properties of planetary atoms,³ the spectra of bound states⁴⁻⁷ and of autoionizing states^{8,9} in external

electric⁴⁻⁹ and magnetic¹⁰ fields, and the exhibition of huge cross sections $\sigma\sim\pi a_0^2n^4$ for chemical reactions such as charge exchange.¹¹ The dynamics of Rydbergs of atoms, diatomic molecules and large molecules is fascinating.⁸⁻⁴⁶ Their radiationless transitions involve atomic autoionization,^{12,13} "reactive" intramolecular dynamics, i.e., molecular predissociation and/or autoionization^{14-16,40-46} and intramolecular "nonreactive" dynamics in a bound level structure, e.g., internal conversion.¹⁷⁻²¹ The partial widths for all the high Rydberg radiationless channels are expected to be determined by the n^3 scaling law,^{14,40-46} which mani-

ffects the normalization of the Rydberg orbital.⁴⁷ The total decay width of a hydrogenic nl Rydberg (where l is the azimuthal quantum number) is expected to be $\Gamma(n) = \Gamma_0(l)/n^3$, where $\Gamma_0(l)$ is an l dependent decay width constant. The total decay width of a molecular or of an atomic ($nIJ\hat{\alpha}$) Rydberg state (with an electronic angular momentum J and other quantum numbers $\hat{\alpha}$), characterized by the quantum defect $\delta(l)$ (which essentially depends on l), is expected to be

$$\Gamma_{IJ\hat{\alpha}}(n) = \Gamma_0(IJ\hat{\alpha})/\nu^3, \quad (1.1)$$

where the effective principal quantum number is $\nu = (n - \delta(l))$ and $\Gamma_0(IJ)$ is a (l and/or J and/or $\hat{\alpha}$ dependent) decay width constant. The dynamics of high ($n = 50-300$) molecular²⁴⁻³⁰ and atomic³¹ Rydbergs, which was interrogated by time-resolved ZEKE (zero electron kinetic energy) spectroscopy²¹⁻³¹ (and are referred to as ZEKE Rydbergs) provided evidence for the breakdown of the n^3 scaling law, Eq. (1.1), which is manifested by

- (a) Long lifetimes of ZEKE Rydbergs of NO. Reiser *et al.*²⁴ have observed high lying (within ~ 10 cm⁻¹ below the ionization potential), very long lived ($\sim \mu$ s lifetimes) Rydbergs of NO. Chupka^{33,34} pointed out that the lifetimes of these states are considerably longer than expected on the basis of n^3 scaling for the predissociative p series of NO.
- (b) The lifetime lengthening of ZEKE Rydbergs of large molecules. The lifetimes of the ZEKE Rydbergs ($n \sim 80-250$) of large molecules²⁶⁻³⁰ are longer by several (2-4) orders of magnitude than those expected on the basis of the n^3 scaling relations. Even, Bersohn and Levine²⁸ have established that the lifetimes of ZEKE Rydbergs ($n \geq 80$) of bis(benzene) chromium (BBC) and of 1,4 diaza bicyclo [2,2,2] octane (DABCO) are longer by 2-3 orders of magnitude than those expected on the basis of Eq. (1.1).
- (c) The lifetime lengthening of ZEKE Rydbergs for various decay channels in atoms, diatomics, and large molecules. The lengthening effect is manifested for internal conversion, predissociation and autoionization in large molecules,²⁶⁻³⁰ for predissociation in diatomic molecules^{24,25} and for autoionization in atoms.^{31,48}

These surprising characteristics of the dynamics of ZEKE Rydbergs triggered extensive theoretical activity.²⁸⁻³⁹ The electric field-induced coupling and mixing model advanced and developed by Chupka,^{33,34} Bordas *et al.*³⁵ Merkt and Zare³⁶ and Jortner and Bixon³⁷ provided an adequate physical picture for the lengthening of the lifetimes of the ZEKE Rydbergs. The energetic and dynamic implications of Stark mixing within high ($n = 50-300$) atomic and molecular ZEKE Rydbergs, which dominate their time-resolved dynamics,³³⁻³⁷ are related to the Stark spectroscopy of both nonreactive and reactive ($n = 10-20$) Rydbergs.⁴⁻¹⁰ Experimental and theoretical studies^{4-7,10} of electric field mixing within nonreactive atomic Rydbergs provided a detailed picture of their Stark maps. In the context of energy-resolved observables for reactive atomic Rydbergs,^{8,9} impressive experimental^{8,9} and theoretical^{8,9} progress was made (using

the Fano line shape formalism¹³ and the quantum defect method⁴⁹) towards the understanding of the Stark absorption lineshapes of the autoionizing Rydbergs of Xe⁽⁸⁾ and of Ar⁽⁹⁾. These line shapes^{8,9} provide information on the autoionization dynamics of ($n = 10-20$) atomic Rydbergs in an electric field. However, this significant energy-resolved information^{8,9} did not explicitly manifest the novel dynamic effects of lifetime lengthening,²⁴⁻³⁹ which was experimentally revealed in the time evolution of the ZEKE Rydbergs. Furthermore, it will be exceedingly difficult to explore the dynamics of high n ($= 100-300$) ZEKE Rydbergs by absorption lineshape studies, in view of spectral congestion effects. Accordingly, one has to resort to the new and interesting area of time-resolved interrogation of ZEKE Rydbergs,²⁴⁻³¹ whose theoretical exploration for atomic autoionization constitutes the theme of this paper.

We pursued³⁷⁻³⁹ the formal analogy between the coupling, accessibility, and decay of high Rydbergs in an external weak ($F = 0.01-1.0$ V/cm) electric field and intramolecular coupling, excitation, and relaxation in a bound level structure.⁵⁰⁻⁵⁷ The effective Hamiltonian formalism was advanced⁵⁴⁻⁵⁷ to treat the dynamics of ultrahigh Rydbergs in a weak electric field.^{37,38} The theory provides a physical picture for the lifetime lengthening of high n Rydbergs in terms of a dilution of low l doorway and escape states within an inactive high l states manifold. The theoretical treatment utilizes as input data quantum defects and decay widths, which are extracted from experiment. From the point of view of general methodology, this approach, which rests on experimental spectroscopic information, is similar to the quantum defect method.⁵⁸ A central result emerging from the analysis is a unified description of the level structure and dynamics of molecular Rydberg predissociation and/or internal conversion and/or (vibrational or rotational) autoionization and of atomic Rydberg autoionization. The universality principle for the level structure and dynamics of high molecular and atomic ZEKE Rydbergs [see point (C) above] is borne out by the experimental observation of the lifetime lengthening of the one-photon excited autoionizing high Rydberg states of Ar first studied by Merkt.³¹ These involve the transitions from the ground state $^1S_0 3p^6$ to the $^2P_{1/2} ns' [1/2]_1$ and the $^2P_{1/2} nd' [3/2]_1$ autoionizing series ($n = 85-200$), which converge to the upper spin-orbit ion state $Ar^+ (^2P_{1/2})$. These states have lifetimes which are more than 50 times longer than those expected for the ns' and nd' states.³¹ These long lifetimes of the ZEKE Rydbergs are attributed to the electric field induced mixing of the doorway states ns' and nd' within the inactive nl ($l > 3$) manifold.^{31,33-38} (For the jl coupling notation for the atomic states used herein, see Appendix A.)

In this paper we present a theoretical study of the dynamics of the $^2P_{1/2} np' [3/2]_1$ autoionizing ZEKE Rydbergs of Ar in weak electric fields, which were experimentally investigated by Mühlfordt and Even in the accompanying paper⁴⁸ by one-photon excitation from the metastable $^2P_{1/2} 4s [3/2]_2$ level. Mühlfordt and Even⁴⁸ reported a dramatic lifetime lengthening effect of the Ar ZEKE np' Rydbergs. A heuristic and admittedly oversimplified single channel analysis of their results will consider the np' state as

doorway and escape state with the widths, Eq. (1.1), $\Gamma_p(n) = 2100/n^3 \text{ (cm}^{-1}\text{)}$.⁴⁸ $\Gamma_p(n)$ constitute a lower limit for the decay widths as the incorporation of nd' escape states (Secs. III and IV) will result in considerably larger widths. The upper limits for the decay lifetimes $\tau(n) = \hbar/\Gamma_p(n)$ are then estimated⁴⁸ to be $\tau(120) \approx 4 \text{ ns}$ and $\tau(200) \approx 20 \text{ ns}$. These estimates are lower by about 2 orders of magnitude than the experimental lifetimes⁴⁸ (e.g., by a numerical factor of ~ 110 for $n=120$ and of ~ 80 for $n=200$). This lifetime dilution effect for the np' ZEKE Rydberg series of Ar is qualitatively similar to the long decay lifetimes of ZEKE Rydbergs of the Ar atom ns' and nd' series³¹ and of large molecules,^{26–30} providing further support for the universality of lifetime lengthening for atomic and molecular ZEKE Rydbergs.

The experimental data^{31,48} for the autoionization dynamics of the ZEKE Rydbergs of Ar will be confronted with the results of the theoretical study based on the multichannel effective Hamiltonian formalism.^{37,38} The gross features of the ZEKE spectra of the autoionizing np' series of Ar explored by Mühlpfordt and Even,⁴⁸ which reveal the lifetime dilution with an onset of the ZEKE peak (for delay times of $t=200\text{--}400 \text{ ns}$) at $n \approx 100$ with a peak of the ZEKE spectrum around $n \approx 250$, are qualitatively similar to those of the ns' and nd' series of Ar previously reported by Merkt.³¹ The onset of the ZEKE spectrum (for a delay time of $t=200 \text{ ns}$) was observed by Merkt³¹ at $n \approx 70\text{--}75$ followed by a gradual increase towards higher n values, a broad peak at $n \approx 120\text{--}180$, and a sharp drop for $n > 180$. The quantitative differences between the experimental results for the np' series⁴⁸ and those for the ns' and nd' series³¹ may originate from extrinsic experimental conditions (e.g., different densities of positive ions existing in the two experiments), as well as from intrinsic effects, i.e., different doorway states in the two experiments. Our analysis will reveal that the gross features of the ZEKE spectra and the lifetime data for the np' series of Mühlpfordt and Even⁴⁸ are accounted for in terms of our multichannel effective Hamiltonian method for l mixing in a homogeneous electric field.^{37,38} The theory succeeds in accounting for some aspects of Merkt's data for the nd' series, i.e., the onset of effective mixing and the near-onset lifetimes.³¹ However, the experimental lifetimes for higher n (≈ 90) nd' Rydbergs are considerably longer than those predicted by us for l mixing, the discrepancy being presumably due to Rydberg–ion collisional induced (lm_i) mixing.^{31,36} We proceed to advance and apply the multichannel effective Hamiltonian formalism^{37,38} for the dynamics of autoionizing Rydbergs.

II. THEORY OF RYDBERG LEVEL STRUCTURE AND DYNAMICS

We shall specify the field-free level structure, the decay widths and the coupling for a high n Rydberg manifold(s) in a weak external electric field. These data provide the input information for the theory of Rydberg dynamics within the framework of the multichannel effective Hamiltonian method.

Consider first the field-free states and their decay widths (Fig. 1). The relevant discrete level structure consists of low

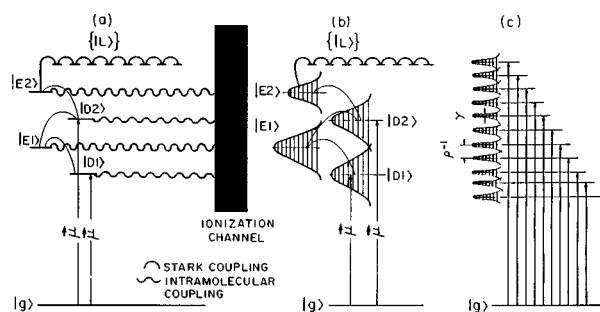


FIG. 1. An energy level scheme for the splitting, mixing, excitation and decay of autoionizing Rydberg states in an external electric field. (a) Several low l doorway states $|D1\rangle$ and $|D2\rangle$ and several low l “pure” escape states $|E1\rangle$ and $|E2\rangle$ are separated from the high l degenerate manifold $\{|L\rangle\}$. The $|D1\rangle$ and $|D2\rangle$ states carry an oscillator strength from the ground state (denoted by a vertical arrow). The $|D1\rangle$, $|D2\rangle$, $|E1\rangle$, and $|E2\rangle$ states are coupled to the ionization channel and constitute escape states for decay. All the discrete states are sequentially Stark coupled by the (weak) electric field. (b) Stark coupling of the eigenstates of the field-free effective Hamiltonian $\mathbf{H}_0 - (i/2)\Gamma$. The doorway and the pure escape states have a partial decay width. The $\{|L\rangle\}$ states in the high l degenerate manifold have zero decay widths. All the states are coupled by the electric field. (c) Mixed independently decaying levels at a finite field. All these levels carry oscillator strengths from the ground state and are characterized by finite decay widths.

l states ($l=0\text{--}3$), which penetrate the core, and a hydrogenic manifold of high l nonpenetrating states ($l>3$). A subset of the low l states constitute the doorway state(s) for excitation. These doorway state(s) are determined by the optical conditions, e.g., one-photon excitation, two-photon excitation or excitation from a metastable intermediate state. All the low l states constitute the escape states for decay. The escape states are coupled to autoionization decay channels and are characterized by decay widths (Fig. 1). The distinction between the doorway and the escape states involves an important feature of the dynamic problem. The doorway state(s) constitute a subset of the escape states. In general, there are $\bar{\alpha}$ doorway states $|D\alpha\rangle$ ($\alpha=1\text{---}\bar{\alpha}$) and $\bar{\beta} + \bar{\alpha}$ escape states, which consist of $|E\beta\rangle$ ($\beta=1\text{---}\bar{\beta}$) “pure” escape states and the doorway states $|D\alpha\rangle$ ($\alpha=1\text{---}\bar{\alpha}$). Finally, the high l (>3) hydrogenic states, which will be denoted by $\{|L\rangle\}$, are inactive in excitation and in decay. The zero-order manifold $\{|\kappa\rangle\}$ consists of the three submanifolds $\{|\kappa\rangle\} \equiv \{|D\alpha\rangle\}$, $\{|E\beta\rangle\}$ and $\{|L\rangle\}$ (Fig. 1). The energies $E(\kappa)$ of these states are $E(\kappa) = IP - R/(n - \delta(\kappa))^2$ with the quantum defects $\{\delta(D\alpha)\}$ for the doorway state(s), $\{\delta(E\beta)\}$ for the other escape states and $\delta(L)=0$ for the inactive manifold. The decay widths $\{\Gamma_\kappa(n)\}$ are characterized by the decay width constants $\{\Gamma_0(D\alpha)\}$ for the doorway state(s), $\{\Gamma_0(E\beta)\}$ for the pure escape states and $\Gamma_0(L)=0$ for the inactive manifold. For atomic autoionization of heavier rare gases (Ar, Kr, Xe) the quantum defects $\delta(\kappa)$ are determined mainly by the azimuthal quantum number l , while the zero-order decay width constants $\Gamma_0(\kappa)$ are determined by the quantum numbers l , K , and J .^{59–63} The decay widths given by the scaling law, Eq. (1.1), are $\Gamma_\kappa(n) = \Gamma_0(\kappa)/(n - \delta(\kappa))^3$.

In the presence of a weak homogeneous electric field F , the Rydberg level structure and dynamics are determined by the effective Hamiltonian^{37,38}

$$\mathbf{H}_{\text{eff}} = \mathbf{H}_0 + \mathbf{H}_{\text{STARK}} - (i/2)\Gamma, \quad (2.1)$$

where \mathbf{H}_0 is the diagonal field-free Hamiltonian for the discrete level structure with the energy levels $E(\kappa)$ which are obtained from the experimental quantum defects. $\mathbf{H}_{\text{STARK}}=eFz$ is the Stark Hamiltonian, with the coupling between the $\{|\kappa\rangle\}$ states being determined by the appropriate selection rules. $\mathbf{\Gamma}$ is the decay matrix for all the $\{|D\alpha\rangle\}$ and $\{|E\beta\rangle\}$ doorway and pure escape states. In general, $\mathbf{\Gamma}$ is off-diagonal. The diagonal matrix elements $\Gamma_\kappa(n)$ of $\mathbf{\Gamma}$ can be inferred for the distinct atomic lKJ states from the experimental line broadening data for the low n Rydbergs using the scaling law, Eq. (1.1). Intelligent guesses for the magnitude of the off-diagonal matrix elements of $\mathbf{\Gamma}$ can be obtained from the diagonal matrix elements and by invoking appropriate conservation rules, e.g., total angular momentum (J) conservation.

The effective Hamiltonian (2.1) can be diagonalized by a complex orthogonal transformation, resulting in the independently decaying levels of the system (Fig. 1)

$$|j\rangle = \sum_{\alpha=1}^{\bar{\alpha}} a_\alpha^{(j)} |D\alpha\rangle + \sum_{\beta=1}^{\bar{\beta}} a_\beta^{(j)} |E\beta\rangle + \sum_L b_L^{(j)} |L\rangle, \quad (2.2)$$

where $\{a_\alpha^{(j)}\}$, $\{a_\beta^{(j)}\}$, and $\{b_L^{(j)}\}$ are (complex) coefficients. The (complex) eigenvalues of the system are

$$\epsilon_j = E_j - (i/2)\gamma_j, \quad (2.3)$$

where E_j are the energy levels and γ_j the decay widths of the $|j\rangle$ eigenstates. The essential input parameters required for the construction of the effective Hamiltonian at a constant field F are (i) the quantum defects $\delta(D\alpha)$ and $\delta(E\beta)$, extracted from the Rydberg series energetics, and (ii) the decay width constants $\Gamma_0(D\alpha)$ and $\Gamma_0(E\beta)$, obtained from the linewidths of the lower Rydberg levels. Thus our theoretical analysis of the dynamics of ultrahigh Rydbergs in weak electric fields rests on the utilization of experimental data.

We shall be concerned with the optical excitation and the decay of the mixed level structure, Eq. (2.2), of a single high n or several high n manifold(s) subjected to l mixing. To make contact with experiment we consider the excited-state total population probability $P(t)$. This corresponds to the time-dependent population of the entire Rydberg manifold. For a broadband excitation of a sparse mixed level structure the time dependent population probability is^{37,38}

$$P(t) = \sum_j \left| \sum_{\alpha=1}^{\bar{\alpha}} a_\alpha^{(j)} \mu_\alpha \right|^2 \exp(-\gamma_j t/\hbar), \quad (2.4)$$

where μ_α is the transition amplitude for the excitation of the doorway state $|D\alpha\rangle$. We note in passing that no temporal coherence effects, i.e., quantum beats in the total decay probability are exhibited.³⁷ The coefficients of each exponential temporal decay term in $P(t)$ involves a superposition of the amplitudes of the doorway states in $|j\rangle$, Eq. (2.2). When more than one doorway state is effectively involved, energetic interference effects can be exhibited.

The theoretical result for $P(t)$,^{37,38} Eq. (2.4), makes contact with reality, being related to the experimental observables interrogated by the time resolved ZEKE spectroscopy:^{22-31,48}

- (1) The ZEKE spectrum is given by the dependence of $P(t)$ at a constant delay time t on the photon excitation energy.
- (2) The time-resolved total population probability corresponds to the delay time t dependence of $P(t)$.
- (3) Lifetimes of ZEKE Rydbergs can be inferred from the time scales for the temporal decay and from the average lifetimes for the decay of $P(t)$.

The two complementary conditions for the validity of Eq. (2.4) are (i) Energetic spread of a single Stark manifold. This is insured when $\Delta\omega_p > \Delta W$ where $\Delta W = 6Rn^2(F/5.15 \times 10^9)$ is the energetic spread of the Rydberg manifold, i.e., $\Delta W = 1.3 \times 10^{-4} n^2 (F/V \text{ cm}^{-1})$. $\Delta\omega_p = 0.1 - 1.0 \text{ cm}^{-1}$ is the spectral width for conventional multimode lasers currently employed in these experiments.^{22-31,48} This condition is obeyed for lower n values, e.g., for $F = 0.05 \text{ V/cm}$ $n \leq 220$ (for $\Delta\omega_p = 0.3 \text{ cm}^{-1}$) and $n \leq 130$ (for $\Delta\omega_p = 0.1 \text{ cm}^{-1}$). (ii) Overlap between Stark manifolds. When $\Delta W/2 > 2R/n^3$ intermanifold overlap prevails, being exhibited for $n > 80F^{-1/5}$. For $F = 0.05 \text{ V/cm}$ this condition is realized for $n > 145$. This intermanifold overlap insures the validity of Eq. (2.4) for high values of n .

Our calculations for the autoionization dynamics of Ar were performed as follows:

- (1) The construction of the multichannel effective Hamiltonian (Secs. III A and III B) for the autoionization of the Ar via the doorway states of the $^2P_{1/2}np'[3/2]_1$ series (Sec. IV) and via the doorway states of the $^2P_{1/2}nd'[3/2]_1$ series (Appendix B).
- (2) The analysis of the dynamics in the limit of strong mixing, which rests on the diagonal sum rule⁵⁴⁻⁵⁷ for the multichannel effective Hamiltonian.
- (3) The diagonalization of the effective Hamiltonian for $n = 50 - \bar{n}$ resulting in the decay widths γ_j and the (single) doorway states amplitudes $a_\alpha^{(j)}$. The upper limit n^- of n was constrained by the onset of field-induced ionization⁵⁹ (in the background field F), which is given by $(IP - \bar{\eta}F^{1/2})$, with⁴⁷ $\bar{\eta} = 6 \text{ cm}^{-1} (\text{V/cm})^{-1/2}$. Neglecting negligible tunneling effects in field ionization,⁴⁷ the upper limit of n is $\bar{n} = (R/\bar{\eta}F^{1/2})$, being $\bar{n} = 240$ for $F = 0.1 \text{ V/cm}$, $\bar{n} = 280$ for $F = 0.05 \text{ V/cm}$ and $\bar{n} = 350$ for $F = 0.02 \text{ V/cm}$.
- (4) The calculation of $P(t)$, Eq. (2.4).

III. THE DYNAMICS OF Ar AUTOIONIZATION

A. Input data

The construction of the effective Hamiltonian, Eq. (2.1) for the autoionization of Ar requires experimental information on the quantum defects and the decay widths parameters of the doorway and the other escape states, which correspond to the ($l=0-3$) ns' , np' , nd' , and nf' manifolds. For the inactive $\{|L\rangle\}$ ($l \geq 4$) Rydbergs $\delta(L) = 0$ and $\Gamma_0(L) = 0$. On the basis of the detailed exploration by Wang and Knight⁶ of the δ and Γ_0 parameters for the autoionizing states of the Xe and the Γ_0 data of Berkowitz^{60,61} and of Wu *et al.*⁶² for the $nd'[3/2]_1$ states of the heavier rare gases, we infer that for

TABLE I. Quantum defects δ and decay width constants Γ_0 for the autoionizing Rydberg series of Ar.

Rydberg series	δ	Γ_0 (cm ⁻¹)
$^2P_{1/2}ns'[1/2]_1$	2.15 ^a	510 ^a
$^2P_{1/2}ns'[1/2]_0$	2.14 ^a	790 ^a
$^2P_{1/2}np'[3/2]_1$	1.68 ^b	2100 ^b
$^2P_{1/2}np'[1/2]_0$	(1.68) ^c	(2100) ^c
$^2P_{1/2}np'[1/2]_1$	(1.68) ^c	(2100) ^c
$^2P_{1/2}np'[3/2]_2$	(1.68) ^c	(2100) ^c
$^2P_{1/2}nd'[3/2]_1$	0.18 ^{d,a}	31 000 ^f
$^2P_{1/2}nd'[3/2]_2$	(0.18) ^e	(10 000) ^g
$^2P_{1/2}nd'[5/2]_2$	(0.18) ^e	(4000) ^g
$^2P_{1/2}nd'[5/2]_3$	(0.18) ^e	(5000) ^g
$^2P_{1/2}nf'[5/2]_2$	0.014 ^d	(100) ^h

^aD. Klar, K. Harth, J. Ganz, T. Kraft, M.-W. Ruf, H. Hotop, V. Tsemekhman, K. Tsemekhman, and M. Ya. Amusia, *Z. Phys. D*, **23**, 101 (1992).

^bA. Mühlpfordt and U. Even, *J. Chem. Phys.* **103**, 4427 (1995).

^cTaken to be identical to the δ and Γ_0 data for $^2P_{1/2}np'[3/2]_1$.

^dK. Yoshino, *J. Opt. Soc. Am.* **60**, 1220 (1970).

^eTaken to be identical to the δ data for $^2P_{1/2}nd'[3/2]_1$.

^fJian Z. Wu, S. B. Whitfield, C. D. Caldwell, M. O. Krause, P. van der Meulen, and A. Fahlman, *Phys. Rev. A* **42**, 1350 (1990).

^gBased on the data for Xe [Liang-guo Wang and R. D. Knight, *Phys. Rev. A* **34**, 3902 (1986)] with a correcting factor of 31/35.

^hRough estimate based on NO data (Ref. 16).

the relevant states of Ar: (i) The quantum defects are essentially determined by l , being only weakly dependent on K and J ; (ii) The decay width constants for the $^2P_{1/2}ns'[1/2]_0$ and for the $^2P_{1/2}ns'[1/2]_1$ states do not strongly depend on K and J ; (iii) The decay width constants for the $^2P_{1/2}nd'[K]_J$ states strongly depend on K and J ; (iv) The $\Gamma_0(nd'[3/2]_1)$ width parameters of Ar and Xe differ only by a numerical factor of ~ 0.89 . The available experimental data for the quantum defects of Ar are taken from the works of Yoshino,⁶³ Radler and Berkowitz,^{60,61} and Klar *et al.*⁶⁴ and from the present work (Table I). The available experimental data for the Γ_0 are taken from Klar *et al.*,⁶⁴ Radler and Berkowitz,^{60,61} Wu *et al.*,⁶² and from the present work (Table I). In the absence of information, we have assumed that the δ and Γ_0 parameters for the $np'[1/2]_{0,1}$ and $np'[3/2]_2$ are identical to those for $^2P_{1/2}np'[3/2]_1$. The δ parameters for the $^2P_{1/2}nd'[3/2]_2$ and the $^2P_{1/2}nd'[5/2]_{2,3}$ states were taken to be identical to those for $^2P_{1/2}nd'[3/2]_1$ [point (i)]. The Γ_0 parameters for the $nd' J=2$ and $J=3$ states of Ar were inferred on the basis of point (iv) from the experimental Γ_0 data for Xe,⁶ which were scaled by the numerical factor of 0.89. The quantum defect for the $^2P_{1/2}nf'[5/2]_2$ series was taken from absorption (quadrupole) spectroscopy,⁶³ while Γ_0 , which is expected to be small for these weakly penetrating orbitals, was roughly estimated from the Rydberg spectroscopy of NO^{15,16} to be $\Gamma_0(f') \leq 100$ cm⁻¹. In Table I we summarize the input data for handling the autoionization dynamics of Ar.

B. Stark coupling

The selection rules for the Stark Hamiltonian $H_{\text{STARK}} = eFz$ are identical to those for dipole transitions. The selection rules in the jl coupling scheme are

$$\Delta M = 0, \quad \Delta S = 0, \quad \Delta j = 0,$$

$$\Delta J = 0, \mp 1 \quad \text{for } |M| = 1 \quad \text{and} \quad \Delta J = \mp 1 \quad \text{for } M = 0, \quad (3.1)$$

$$\Delta K = 0, \mp 1, \quad \Delta l = \mp 1.$$

Introducing the effective principal quantum number ν , the standard angular momentum algebra leads to the following matrix elements for the Stark coupling:^{5,8}

$$\begin{aligned} &\langle (\nu l j) K s J M | z | (\nu' l' j) K' s J' M \rangle \\ &= (-1)^{J+J'+K+K'+l+j+s-M}, \\ &[(2J+1)(2J'+1)(2K+1)(2K'+1)]^{1/2} \begin{pmatrix} J & 1 & J' \\ -M & 0 & M \end{pmatrix} \\ &\times \begin{Bmatrix} K & J & s \\ J' & K' & 1 \end{Bmatrix} \begin{Bmatrix} l & K & j \\ K' & l' & 1 \end{Bmatrix} \langle \nu l | r | \nu' l' \rangle \end{aligned} \quad (3.2)$$

with

$$\langle \nu l | r | \nu' l' \rangle = \begin{cases} -\sqrt{l+1} \langle \nu l | r | \nu' l+1 \rangle, & l' = l+1 \\ \sqrt{l} \langle \nu l | r | \nu' l-1 \rangle, & l' = l-1 \end{cases} \quad (3.3)$$

For a given value of the principal quantum number n one has a manifold of states of dimension $4n-2$, which is mixed by the coupling. In the special case $M=0$, due to the restricted selection rule $\Delta J = \mp 1$ ($\Delta J \neq 0$), the manifold of states decomposes into two noninteracting submanifolds: $J=l$ and $J=l \mp 1$.

The radial matrix elements in Eq. (3.3) are evaluated for different quantum defects [which give l dependent effective principal quantum number $\nu = n - \delta(l')$], using the formula of Edmonds *et al.*⁶⁵

$$\langle \nu l | r | \nu' l' \rangle = \left[\frac{3}{2} \nu_c^2 \left(1 - \left(\frac{l_c}{\nu_c} \right)^2 \right)^{1/2} \right] \sum_{\mu=0}^3 \gamma^\mu g_\mu(\Delta \nu), \quad (3.4)$$

where

$$\begin{aligned} l_c &= \max(l, l'), \quad \nu_c = \frac{2\nu\nu'}{(\nu + \nu')}, \quad \Delta l = (l - l'), \\ \gamma &= \Delta l \left(\frac{l_c}{\nu_c} \right), \quad \Delta \nu = \nu - \nu'. \end{aligned} \quad (3.4a)$$

The functions $g_\mu(\Delta \nu)$ were tabulated by Edmonds *et al.*⁶⁵

The selection rules, Eq. (3.1), together with the experimental input information (Table I) and the matrix elements (3.2)–(3.4), enable the construction of the multichannel effective Hamiltonian. A single Rydberg manifold employed in our calculations (which will be referred to as a single n manifold), will be chosen to contain a set of zero-order states with the closest ν values. Such a single n manifold will be characterized as follows: (1) The nl hydrogenic states for the $\{[L]\}$ submanifold. (2) The νl ($\nu = n - [(2\delta(l))(\text{mod}1) - \delta(l)(\text{mod}1)]$) doorway and escape states for which $\delta(l) \neq 0$. These latter states correspond to the principal quantum number $n'' = n + \delta(l) - \delta(l)(\text{mod}1)$.

Armed with these results we proceed to explore the autoionization dynamics of the $^2P_{1/2}np'[3/2]_1$ Rydberg states, which were studied by Mühlpfordt and Even.⁴⁸ The theoretical treatment of the autoionization of the $^2P_{1/2}ns'[1/2]_1$

and ${}^2P_{1/2}nd'[3/2]_1$ manifolds one-photon excited from the ${}^1S_03p^6$ ground state, which were experimentally studied by Merkt,³¹ will be presented in Appendix B.

IV. AUTOIONIZATION DYNAMICS FOR THE RYDBERG MANIFOLDS EXCITED VIA THE ${}^2P_{1/2}np'[3/2]_1$ DOORWAY STATE

A. Doorway state, other escape states and the inactive manifold

We shall focus on the dynamics of high Rydberg states, which are one-photon excited from the metastable ${}^2P_{3/2}4s[3/2]_2$ state.⁴⁸ The selection rules dictate excitations to the following four np' and nf' series:^{61,66,67} ${}^2P_{1/2}np'[3/2]_1$, ${}^2P_{1/2}np'[1/2]_1$, ${}^2P_{1/2}nf'[5/2]_3$, and ${}^2P_{1/2}nf'[7/2]_3$. In the experimental spectrum of Even and Mühlpfordt, the two ${}^2P_{1/2}np'[3/2]_1$ and ${}^2P_{1/2}nf'[5/2]_3$ series are exhibited,⁴⁸ with similar amplitudes (i.e., the low-resolution amplitudes of the np' series are lower by a numerical factor of ~ 2 than those for the nf' series). However, the resonance widths are considerably different. While for

the np' series the resonance widths are large $\Gamma_0(p')=2100\text{ cm}^{-1}$,⁴⁸ the decay width parameters $\Gamma_0(f')$ of the weakly penetrating nf' series are small, i.e., $\Gamma_0(f')\leq 100\text{ cm}^{-1}$ (Table I). Accordingly, the oscillator strength for the excitation of a nf' state is lower by more than 1-order-of-magnitude than for the np' state with the same n , whereupon the overwhelming largest transition probability is to the ${}^2P_{1/2}np'[3/2]_1$ series. For a given n manifold, the ${}^2P_{1/2}np'[3/2]_1$ state constitutes the doorway state, as well as one of the escape states. The other relevant pure (low l) escape states are those states with $l\leq 3$, which are coupled directly, or indirectly to the doorway state.

B. The effective Hamiltonian

The doorway state ${}^2P_{1/2}np'[3/2]_1$ corresponds to a triplet manifold and we shall take its $M=0$ component. The effective Hamiltonian matrix for this system couples the $2n-1$ atomic states for which $J=l$ and $K=l\pm 1/2$. Its schematic structure is represented in the form

$$\begin{array}{cccccccc}
 s'[1/2]_0 & \exists & \exists & 0 & 0 & 0 & 0 & 0 \\
 \exists & p'[1/2]_1 & 0 & \exists & 0 & 0 & 0 & 0 \\
 \exists & 0 & p'[3/2]_1 & \exists & \exists & 0 & 0 & 0 \\
 0 & \exists & \exists & d'[3/2]_2 & 0 & \exists & 0 & 0 \dots \\
 0 & 0 & \exists & 0 & d'[5/2]_2 & \exists & \exists & 0 \\
 0 & 0 & 0 & \exists & \exists & f'[5/2]_3 & 0 & \exists \\
 0 & 0 & 0 & 0 & \exists & 0 & f'[7/2]_3 & \exists \\
 0 & 0 & 0 & 0 & 0 & \exists & \exists & g'[7/2]_4 \\
 & & & & \vdots & & & \ddots
 \end{array} \tag{4.1}$$

The diagonal elements in Eq. (4.1) are designated by the corresponding atomic terms (in the jl coupling scheme). The selection rules, Eq. (3.1), determine the nonzero off-diagonal elements, which are represented by \exists in Eq. (4.1). The diagonal and nonzero off-diagonal elements of the effective Hamiltonian are obtained by using the following prescriptions:

- (1) Each of the first seven diagonal elements, which represent the doorway and escape states, is given by $-R/\nu^2 - (i/2)\Gamma_0(IKJ)/\nu^3$ with $\nu = n - [(2\delta(l)\bmod 1) - (\delta(l)\bmod 1)]$.
- (2) All the other diagonal matrix elements, which represent the $\{L\}$ submanifold, are given by $-R/n^2$.
- (3) Each off diagonal element is given by Eqs. (3.2) and (3.3), which will be now expressed in an explicit form.

For the $M=0$ ($J=l$) manifold the Stark couplings between l and $l+1$ ($\Delta S=\Delta M=\Delta j=0$) are given by Eqs. (3.2) and (3.3) and have the forms:

For $K=l-1/2$, $J=l$ $\{\Delta K=\Delta J=\Delta l=1\}$:

$$\langle J,K,l|z|J+1,K+1,l+1\rangle = \frac{[l(l+1)]^{1/2}}{2l+1} \langle \nu l|r|\nu' l+1\rangle, \tag{4.2a}$$

for $K=l+1/2$, $J=l$ $\{\Delta K=0, \Delta J=\Delta l=1\}$:

$$\langle J,K,l|z|J+1,K,l+1\rangle = \frac{1}{(2l+1)(2l+3)} \langle \nu l|r|\nu' l+1\rangle, \tag{4.2b}$$

and for $K=l+1/2$, $J=l$ $\{\Delta K=\Delta J=\Delta l=1\}$:

$$\langle J,K,l|z|J+1,K+1,l+1\rangle = \left[\frac{(l+1)}{2(2l+3)} \right]^{1/2} \langle \nu l|r|\nu' l+1\rangle. \tag{4.2c}$$

The radial matrix elements in Eq. (4.2) for large values of n and for finite quantum defects are obtained from Eqs. (3.4) and (3.4a) in the form⁶⁵

$$\begin{aligned}
 \langle \nu l|r|\nu'(l+1)\rangle &= 3/2\nu_c^2 a_0 [1 - (l+1)^2/\nu_c^2]^{1/2} \{g_0(\Delta\nu) \\
 &+ [(l+1)/\nu_c]g_1(\Delta\nu) + \dots\}. \tag{4.3}
 \end{aligned}$$

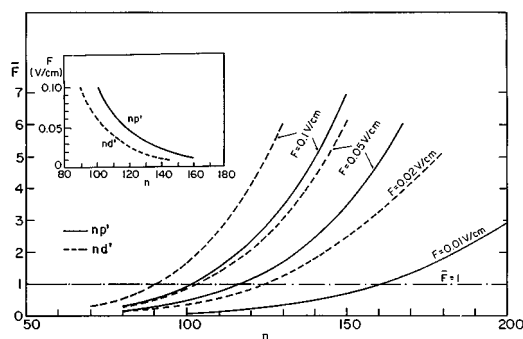


FIG. 2. The n dependence of the reduced electric field $\bar{F}(n, l')$ for $l' = 1$ and 2 for several strengths of the electric field (F) marked on the figure. The horizontal line ($\bar{F} = 1$) denotes the onset of effective mixing. The insert shows the n values for which effective mixing sets in for different values of F (marked on the figure).

The effective Hamiltonian is constructed using prescriptions (1)–(3) and the data of Table I, together with Eqs. (4.2) and (4.3). \mathbf{H}_{eff} contains the entire contributions of \mathbf{H}_0 and $\mathbf{H}_{\text{STARK}}$ and the diagonal terms of the decay matrix $(i/2)\mathbf{\Gamma}$ in Eq. (2.1). This effective Hamiltonian with the diagonal decay matrix neglects some possible coherent effects in the decay. These originate from the contribution of off-diagonal elements of $\mathbf{\Gamma}$, which are subjected to angular momentum conservation. We shall show in Sec. VII E that the contribution of these off-diagonal matrix elements to $P(t)$ is small. We shall now apply the effective Hamiltonian formalism for the autoionization dynamics of the $^2P_{1/2}nl'$ manifolds populated via the $^2P_{1/2}np'[3/2]_1$ ($M=0$) doorway state. We shall start with the limit of strong mixing, where the application of the diagonal sum rule for the effective Hamiltonian is sufficient to provide semiquantitative information on the dynamics and then proceed to the full diagonalization of the effective Hamiltonian.

C. Strong mixing

According to Eq. (4.1) we are concerned with the one doorway (and escape) state $^2P_{1/2}np'[3/2]_1$ and with six pure escape states for each value of n . A cursory examination of the structure of \mathbf{H}_{eff} for the problem, together with the data of Table I, reveals that the decay is dominated by the doorway (and escape) $np'[3/2]_1$ state, together with the three $np'[1/2]_1$, $nd'[3/2]_2$ and $nd'[5/2]_2$ pure escape states, which are characterized by the largest values of the decay widths. We have to focus on the effective field induced mixing of these np' and nd' states with the inactive manifold. The condition for the onset of effective mixing of an nl' Rydberg [with a quantum defect $\delta(l')$] with the inactive $\{|L\rangle\}$ manifold and with other nl'' states [which are characterized by $\delta(l'')(\text{mod}1) < \delta(l')(\text{mod}1)$] is specified by the condition

$$\bar{F}(n, l') \geq 0.5 - 1, \quad (4.4)$$

where the homogeneous electric field in reduced units is

$$\bar{F}(n, l') = (F/\text{V cm}^{-1})n^5/3.4 \times 10^9 [\delta(l')(\text{mod}1)]. \quad (4.5)$$

In Fig. 2 we present convenient plots of $\bar{F}(n, l')$ vs n for the

relevant nd' and np' series. As $\delta(p')(\text{mod}1) > \delta(d')$, the condition (4.4) for effective mixing is determined by $\bar{F}(n, p') \geq 1$. The np' doorway and escape states exhibit the onsets of effective mixing with the inactive $\{|L\rangle\}$ manifold and with the other nd' escape states ($\bar{F}(p') > 1$) in the range $n = 140 - 195$ for reasonable values of the weak stray field $F = 0.1 - 0.02$ V/cm (see insert to Fig. 2).

Strong mixing of the doorway, escape and inactive states is realized when $\bar{F}(n, l') \geq 1$. Our numerical calculations show that for the Ar autoionization dynamics strong mixing is realized with

$$\bar{F}(n, p') \geq 3. \quad (4.6)$$

We can now utilize the diagonal sum rule^{54–56} for the condition of strong mixing, Eq. (4.6). The diagonal sum rule for the effective Hamiltonian, Eq. (4.1), is

$$\sum_{j=1}^{2n-1} \gamma_j = \sum_{(IKJ)} \Gamma_0(IKJ)/(n - \delta(I))^3, \quad (4.7)$$

where the sum on the RHS of Eq. (4.7) is taken over all the contributing doorway and escape states. In the limit of large n we can set

$$\sum_{j=1}^{2n} \gamma_j = \Gamma_0^T/n^3, \quad (4.8)$$

where

$$\Gamma_0^T = \sum_{(IKJ)} \Gamma_0(IKJ). \quad (4.9)$$

We note in passing that relations (4.7)–(4.9) are valid for all field strengths. In the limit of strong mixing democratic admixture of the decay widths of the doorway and escape states is exhibited among all the $|j\rangle$ eigenstates. The average decay width $\langle \gamma(n) \rangle$ of each mixed state within a single n manifold is $\langle \gamma(n) \rangle = (2n)^{-1} \sum_j \gamma_j$. Accordingly, $\langle \gamma(n) \rangle \approx \Gamma_0^T/2n^4$ and the average decay lifetime $\langle \tau_{\text{SM}}(n) \rangle = \hbar/\langle \gamma(n) \rangle$ for strong mixing (SM) is given by

$$\langle \tau_{\text{SM}}(n) \rangle \approx 2n^4 \hbar / \Gamma_0^T. \quad (4.10)$$

The approximation (4.10) is expected to be valid for n and F values, which satisfy the condition $\bar{F}(n, l' = 1) \geq 3$. In this strong mixing domain the population probability is approximately given by

$$P_{\text{SM}}(t) \approx \exp(-t/\langle \tau_{\text{SM}}(n) \rangle). \quad (4.11)$$

From Eq. (4.9) and the data in Table I we obtain $\Gamma_0^T = 19\,100 \text{ cm}^{-1}$. Making use of Eq. (4.7) we present in Fig. 3 the n dependence of $\langle \tau_{\text{SM}}(n) \rangle$ in the strong mixing limit. We have also marked in Fig. 3 the onsets of the strong mixing limit for $F = 0.02 - 0.1$ V/cm. The approximate n dependence of $P_{\text{SM}}(t)$ for a fixed t vs n , which represents the ZEKE spectra for $t = 200$ ns and $t = 400$ ns, are also presented in Fig. 3.

Equations (4.10) and (4.11) provide a useful approximation for the ZEKE Rydberg dynamics for strong mixing. Nevertheless, these results are approximate and of somewhat limited applicability [$\bar{F}(n, p') > 3$]. The decay lifetimes even in the strong mixing limit are not strictly exponential.

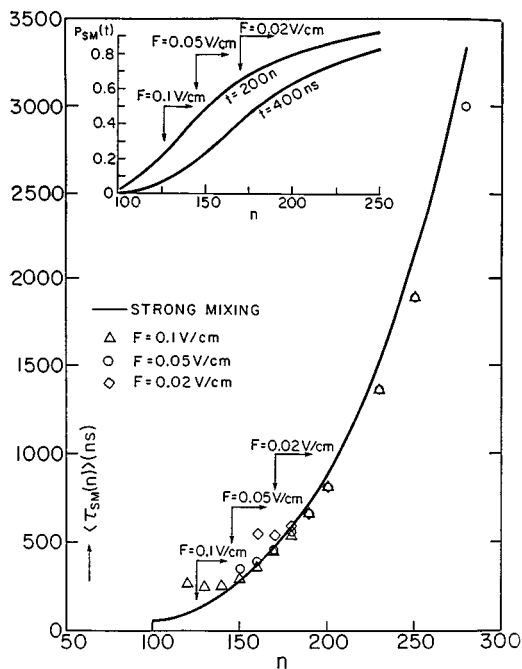


FIG. 3. The n dependence of the lifetime $\langle \tau_{SM}(n) \rangle$ in the strong mixing limit, Eq. (4.10), for $n=100-280$ (${}^2P_{1/2}np'[3/2]_1$ doorway state). The points (Δ , \circ , and \diamond) represent the numerical results for the (averaged) decay lifetimes for the decay of $P(t)$ in the range $t=200-1000$ ns, which were obtained from the diagonalization of the multichannel effective Hamiltonian (for $F=0.1, 0.05$, and 0.02 V/cm). The perpendicular arrows mark the onsets of the strong mixing for different values of n (marked on the arrows). The insert shows the n dependence of the total population probability in the strong mixing limit for $t=200$ ns and $t=400$ ns.

More important, for weaker fields, i.e., $\bar{F}(n, p') < 1$ a hierarchy of two time scales³⁸ is exhibited for the lifetimes, manifesting the failure of Eqs. (4.10) and (4.11). Thus, in the low range of F values, for relatively low $n \approx 100$ and for short times, the theory has to be extended by the diagonalization of the effective Hamiltonian, Eq. (4.1)

D. Calculations

We have diagonalized the multichannel effective Hamiltonian with the ${}^2P_{1/2}np'[3/2]_1$ ($M=0$) doorway state for single n manifolds with the input information of Secs. IV A, IV B and Table I. The calculations were performed for $n=80-280$ and for $F=0.02-1.0$ V/cm. The following numerical data were obtained: (i) the energies E_j of the $\{|j\rangle\}$ states (Sec. II), (ii) the decay widths γ_j and lifetimes $\tau_j = \hbar/\gamma_j$ of the $\{|j\rangle\}$ states and (iii) the mixing coefficients $|a_\alpha^{(j)}|^2$ of the (single) doorway state $\alpha \equiv np'[3/2]_1$ within all the $|j\rangle$ states. From these data we have constructed the lifetime spectra (τ_j vs E_j), the accessibility spectra ($|a_\alpha^{(j)}|^2$ vs E_j) and the lifetime-accessibility maps ($|a_\alpha^{(j)}|^2$ vs τ_j).

Typical results for the lifetime spectra and the accessibility spectra for the $n=150$ manifold at several electric fields are presented in Fig. 4. Both the lifetime and the accessibility spectra reveal two branches, which manifest the structure of the coupling within the $(2n-1)$ dimensional effective Hamiltonian. The coupling between the two submanifolds $K=l-1/2$ and $K=l+1/2$ is weak, as compared to the intrasubmanifold coupling. For low values of $F=0.02$

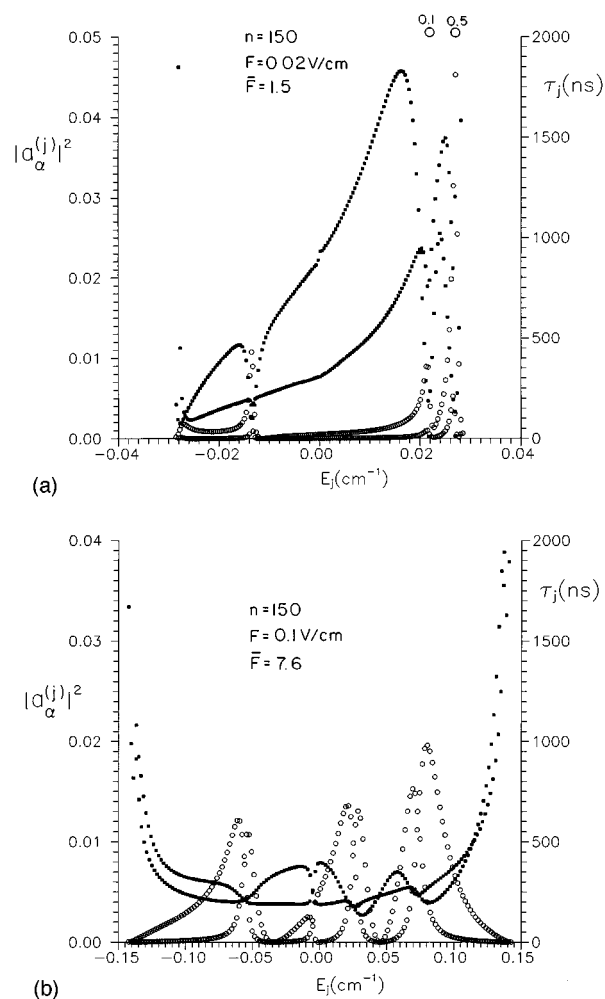


FIG. 4. The lifetime and accessibility spectra for the $n=150$ Rydberg manifold of Ar (${}^2P_{1/2}np'[3/2]_1$ doorway state). (\blacksquare) τ_j vs E_j and (\circ) $|a_\alpha^{(j)}|^2$ vs E_j . (a) $F=0.02$ V/cm ($\bar{F}(150, p')=1.5$). Note the two short ($\tau_j=25$ ns) lifetimes with the large amplitudes ($|a_\alpha^{(j)}|^2=0.5$ and 0.1), which correspond just above the onset of effective mixing. (b) $F=0.1$ V/cm ($\bar{F}(150, p')=7.6$). Strong mixing.

V/cm, which correspond to the onset of the effective mixing of the doorway state $p'[3/2]_1$ and the escape state $p'[1/2]_1$ (i.e., $\bar{F}(150, p')=1.5$), the mixing of the $d'[3/2]_2$ and $d'[5/2]_2$ escape states is large (Fig. 2). The lifetime spectra [Fig. 4(a)] show two short lifetimes at 0.0268 cm^{-1} ($|a_\alpha^{(j)}|^2=0.5$) and at $E_j=0.0215$ cm^{-1} ($|a_\alpha^{(j)}|^2=0.1$), which exhibit the p' doorway state and the p' escape state, respectively. In the lower energy domain of Fig. 4(a), where the mixing of the d' escape states is already extensive, the minimum of $\tau_j \approx 100$ ns at $E_j = -0.013$ cm^{-1} reflects a residue of these d' states. Increasing the electric field to $F=0.1$ V/cm [Fig. 4(b)], the np' mixing becomes strong [i.e., $\bar{F}(150, p')=7.5$], with each of the two branches exhibiting three peaks which correspond (in the order of decreasing energy) to the two doorway and pure escape p' , the escape s' and the two escape nd' states. The lifetimes in the range of large amplitudes [Fig. 4(b)] start converging towards the average value of $\langle \tau_{SM}(150) \rangle = 270$ ns, Eq. (4.10). The lifetime-accessibility maps (Fig. 5) for $F=0.02$ V/cm [$\bar{F}(150, p')=1.5$] and $F=0.1$ V/cm [$\bar{F}(150, p')=7.5$]

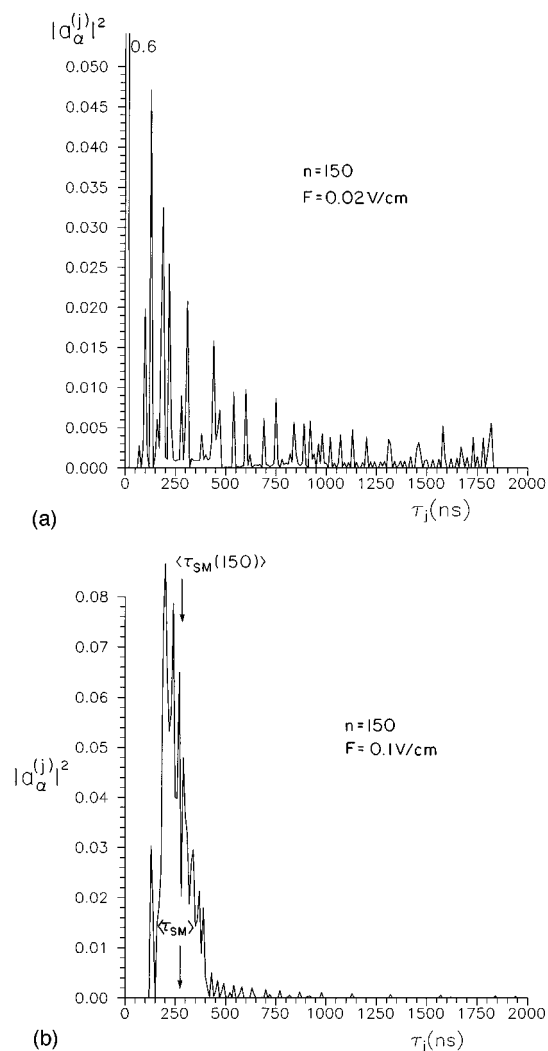


FIG. 5. Lifetime-accessibility maps for $n=150$ Rydberg manifold of Ar ($^2P_{1/2}np'[3/2]_1$ doorway state). (a) $F=0.02$ V/cm. (b) $F=0.1$ V/cm. The value of the strong mixing lifetime $\langle\tau_{SM}(n)\rangle$ is marked by an arrow.

demonstrate the transition from the onset of mixing [Eq. (4.4)] to the situation of strong mixing, Eq. (4.6). For $F=0.02$ V/cm, [Fig. 5(a)], the lifetime-accessibility map for weak p' mixing is characterized by (I) a short lifetime of $\tau_{\text{SHORT}}=25$ ns (with a large amplitude of $|a_\alpha^{(j)}|^2=0.6$), which is close to, but longer than, the lifetime [$\tau = \Gamma_0(p')/n^3$] $\tau=20$ ns of the $(150p'[3/2]_1)$ doorway state (Tables I and II) a very broad distribution of long lifetimes in the range 75–2000 ns with amplitudes $|a_\alpha^{(j)}|^2=0.048$ –0.005. The exhibition of two distinct time ranges [ranges (I) and (II)] for the decay, together with a broad distribution of long lifetimes, is characteristic of the weak coupling situation. The physical situation drastically differs for $F=0.1$ V/cm ($\bar{F}(150,p')=7.5$) [Fig. 5(b)], where strong p' (and d') mixing is exhibited. The lifetime-accessibility map for strong mixing [Fig. 5(b)] reveals a narrow distribution, which peaks around the average value, Eq. (4.10), $\langle\tau_{SM}(150)\rangle=280$ ns, as appropriate for the limit of strong mixing. It is important to notice that even in this limiting case there exist low-amplitude states with much longer lifetimes.

TABLE II. Decay lifetimes for the strong mixing limit for Ar autoionization via the $^2P_{1/2}nd'[3/2]_1$ doorway state.

n	$\bar{F}(n,d')$ ^a	$\langle\tau_{SM}(n)\rangle$ (ns) ^b
60	0.13	3.5
70	0.28	6.5
80	0.55	11
90	1.0	18
100	1.7	27
112	3.0	42
130	6.3	77
150	13	131
200	54	417
240	95	866

^aFor $F=0.1$ V/cm.

^bEquation (4.10).

In Fig. 6 we portray the calculated time evolution of the population $P(t)$ for $F=0.02, 0.05$, and 0.1 V/cm over a range of n values $n=100$ –250. The time resolved decay curves at fixed F (Fig. 6) reveal a transition from a bimodal decay at lower n to long-time nonexponential decay at higher n , exhibiting the two coupling ranges:

Range (A). The range of the onset of effective coupling of the np' doorway and escape states, i.e., $0.7 \leq \bar{F}(n,p') \leq 2$. [In this range the nd' escape states are quite effectively mixed, i.e., $1 \leq F(n,d') \leq 4$.] In this range (Fig. 6) we observe:

(A1) Two distinct time scales for the decay.

(A2) A short lifetime in the range of ~ 20 –100 ns. These short decay times represent the residues of the np' doorway state [Figs. 4(a) and 5(a)].

(A3) A broad distribution of very long decay times, which corresponds to the ineffective mixing of the np' doorway and escape states (and of the nd' states) into the inactive $\{|L\rangle\}$ manifold. The average value $\langle\tau_{\text{LONG}}(n)\rangle$ of the long lifetimes for a given value of n is expected to be considerably longer than the average value $\langle\tau_{SM}(n)\rangle$, Eq. (4.10), for strong democratic mixing at this value of n , i.e., $\langle\tau_{\text{LONG}}(n)\rangle > \langle\tau(n)\rangle$ for $\bar{F}(n,p') \leq 2$. In this range we may set $\langle\tau_{\text{LONG}}(n)\rangle = \eta(n)\langle\tau_{SM}(n)\rangle$, where $\eta(n) > 1$ (≈ 2 –5) is an (n dependent) numerical factor.

(A4) $\langle\tau_{\text{LONG}}\rangle$ decreases with increasing n , reflecting more effective mixing.

Range (B). The strong mixing domain, i.e., $\bar{F}(n,p') \geq 3$. In this domain of sufficiently high n , the two distinct time scales of range (A) collapse into a single long lifetime distribution, which exhibits (Fig. 6)

(B1) A multiexponential slow decay with an average value $\langle\tau\rangle$.

(B2) That the average lifetimes $\langle\tau\rangle$ are well represented by the strong mixing lifetimes $\langle\tau_{SM}(n)\rangle$, Eq. (4.10).

Figure 7 presents the average lifetimes $\langle\tau_{\text{LONG}}\rangle$ [range (A)], and $\langle\tau\rangle$ [range (B)] calculated from the time domain $t=200$ –1000 ns. We also include in Fig. 7 the values of $P(t)$ at $t=600$ ns, which are important to assess the experimental feasibility of the observation of these long lifetimes. For range (A) of the onset of effective coupling these average lifetimes represent the average $\langle\tau_{\text{LONG}}\rangle$ of the long decay

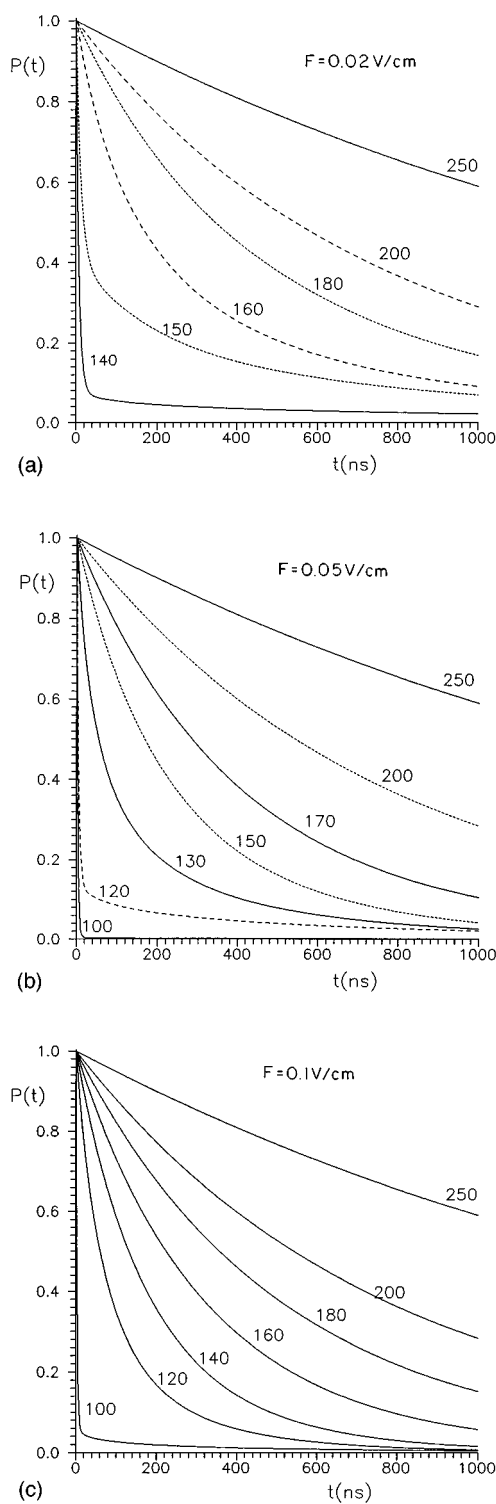


FIG. 6. The time-resolved total population of $n=100-280$ Rydbergs of Ar ($^2P_{1/2}np'[3/2]_1$ doorway state) with the n values marked on curves at different electric field. (a) $F=0.02$ V/cm. (b) $F=0.05$ V/cm. (c) $F=0.1$ V/cm.

component, which decrease with increasing n . In this lower n range (A) the amplitudes of the long-time component of $P(t)$ [marked by $P(t=600$ ns) in Fig. 7] are rather low, i.e., $P(t=600$ ns) ≤ 0.1 , providing an experimental challenge from the observation of these very long lifetimes. For range (B) of strong mixing the lifetimes are nearly independent of

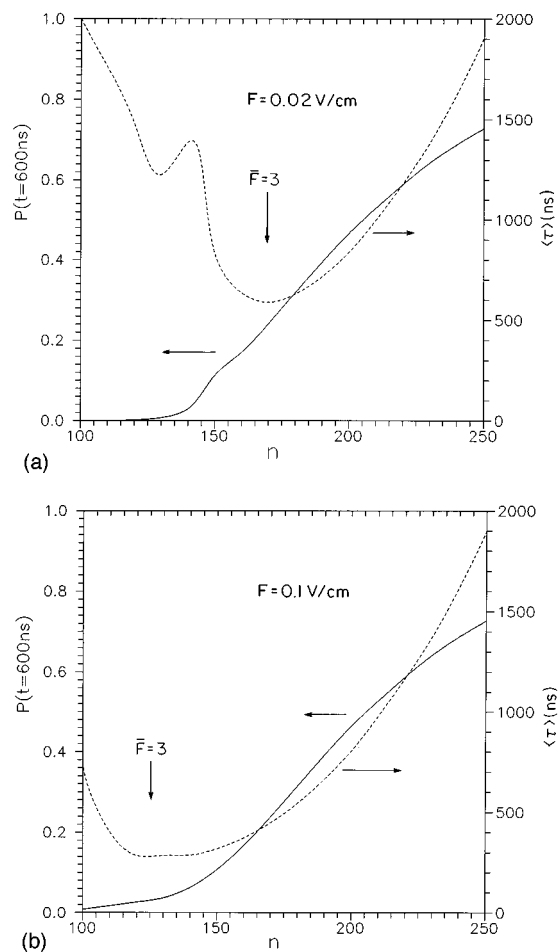


FIG. 7. The n dependence of the average long lifetimes $\langle\tau_{LONG}(n)\rangle$ for range (A) and $\langle\tau(n)\rangle$ for range (B) (dotted lines) and of the population probability at $T=600$ ns (solid lines) for the $np'[3/2]_1$ doorway state. (a) $F=0.02$ V/cm. (b) $F=0.1$ V/cm.

F [see Fig. 7 where we have marked the onset of strong mixing $\bar{F}(n, p')=3$]. As is evident from Fig. 3, the lifetimes in range (B), which are obtained from our numerical calculations of $P(t)$, are well represented by the simple strong mixing result, Eq. (4.10).

Complementary information is obtained from the calculated ZEKE spectra, i.e., the $P(t)$ values at fixed t vs n or vs the energy E (defined relative to IP=0). In Fig. 8 we present the calculated ZEKE spectra for several delay times ($t=60, 200, 400$ ns) at several values of F . At short delay times ($t=60$ ns) a sharp rise of $P(t)$ vs n is exhibited marking the transition from range A (i.e., the long-time low-amplitude component of range A) to range B, with increasing n . For longer delay times ($t=200, 400$ ns) the increase of $P(t)$ spectra with increasing n is more gradual than for the short delays. For lower n values ($n=100-150$) a marked dependence of the spectra on the electric field strength ($F=0.02-0.1$ V/cm) is exhibited with the spectrum moving towards lower n values and rising more gradually with increasing F . These effects manifest the movement of the onsets for effective mixing and for strong mixing towards lower n values with increasing F . For larger values of n (>150) the spectra

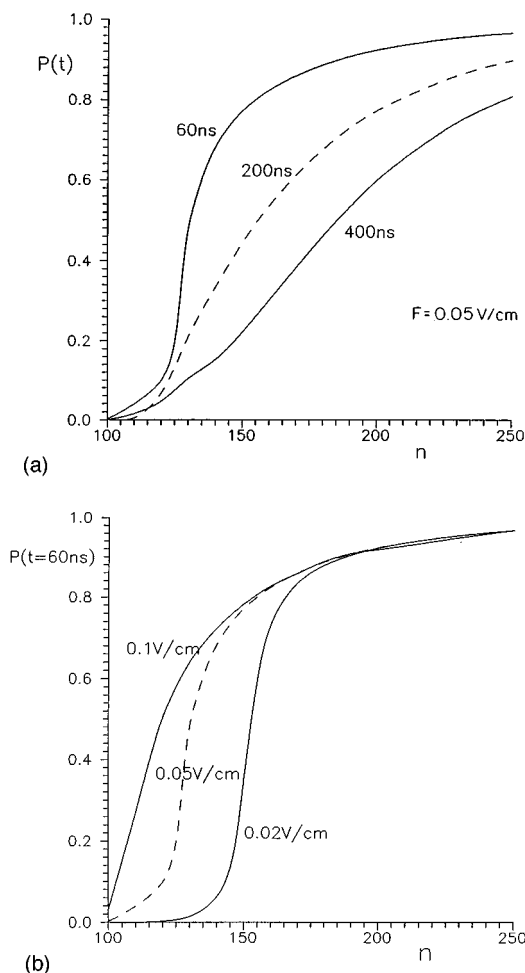


FIG. 8. The calculated ZEKE spectra (${}^2P_{1/2}np'[3/2]_1$ doorway state) ($P(t)$ at fixed t vs n). (a) Delay time dependence $t=60, 200,$ and 400 ns at $F=0.05$ V/cm. (b) Field dependence at fixed $t=60$ ns, $F=0.02, 0.05,$ and 0.1 V/cm.

are practically independent of the electric field strength [Fig. 8(b)], reaching the strong mixing region.

The electric field dependence of the temporal population $P(t)$ vs t for a fixed value of n provides a complementary insight into the transition from range A to range B with increasing F (Fig. 9). For low field $F=0.02$ V/cm [$\bar{F}(150, p')=1.5$] $P(t)$ is characterized by two distinct time scales, with a very long decay component $\langle\tau_{\text{LONG}}\rangle\approx 830$ ns, which reflects effective, but weak mixing. With increasing F to 0.05 V/cm ($\bar{F}=3.8$), the strong mixing situation is realized with a single multiexponential decay component. Of course, the field-induced spectra [i.e., $P(t)$ for fixed t and n vs F] will exhibit either an increase (at shorter $t < 600$ ns) or a decrease (at $t > 600$ ns) with increasing F . The electric field dependence of the average lifetimes, i.e., $\langle\tau_{\text{LONG}}\rangle$ for $F=0.02$ V/cm and $\langle\tau\rangle$ for other values of F in Fig. 9 reflects the shortening of the long lifetime with enhanced mixing. In the range $F\geq 0.05$ V/cm $\langle\tau\rangle$ is weakly field dependent, converging to the value $\langle\tau_{\text{SM}}(150)\rangle=280$ ns, Eq. (4.10) (see insert to Fig. 9), as appropriate for the strong mixing limit.

E. A comment on coherence effects

In our calculations we have used the effective Hamiltonian with the diagonal decay matrix, neglecting the contri-

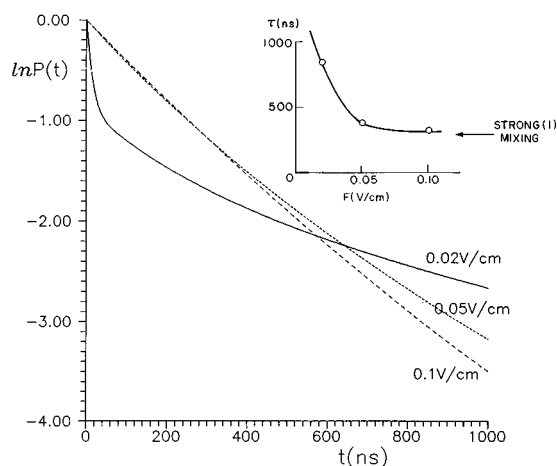


FIG. 9. Electric field dependence of $\ln[P(t)]$ vs t for $n=150$. $F=0.02, 0.05,$ and 0.1 V/cm (marked on the curves) for the ${}^2P_{1/2}np'[3/2]_1$ doorway state. The insert shows the dependence of the long lifetimes on F , with the arrow marking the limit of strong mixing given by $\langle\tau_{\text{SM}}(n)\rangle$, Eq. (4.10).

tribution of off-diagonal elements of Γ . The nonvanishing off-diagonal matrix elements of Γ are subjected to angular momentum conservation. Thus finite off-diagonal terms will appear between pairs of $l'[K]_J$ ($K=l'\pm 1/2$) states with the same value of l' ($3\leq l'\leq 1$). Nothing is known about these off-diagonal matrix elements of Γ , so we make an intelligent guess for the upper limit of (the absolute values of) such elements expressed in terms of the diagonal elements, i.e., $\Gamma(l'[l'+1/2]_J, l'[l'-1/2]_J)\approx[\Gamma(l'[l'+1/2]_J)\Gamma(l'[l'-1/2]_J)]^{1/2}$. In this heuristic description the dominating off-diagonal matrix element connects the $nd'[3/2]_1$ and $nd'[5/2]_2$ states, and its value was taken (Table I) as $6000/n^3$ cm $^{-1}$. Numerical calculations using the off-diagonal effective Hamiltonian revealed that the effect of these off-diagonal matrix elements is minor, e.g., for $n=150$ and 200 at $F=0.05$ V/cm the change in $P(t)$ is smaller than 5% for all values of t . This very weak coherence effect on the dynamics can be readily rationalized in terms of the diagonal sum rule, Eq. (4.7), in the strong mixing situation, Eq. (4.10). In the strong mixing limit the (average) decay times are independent of the off-diagonal elements of Γ .

V. THEORY, EXPERIMENT, AND PERSPECTIVES

The predictions emerging from our theoretical analysis for the autoionization dynamics via the $np'[3/2]_1$ doorway states are

- (1) The identification of the onset of effective mixing and of range (A) ($0.7\leq\bar{F}(n, p')\leq 1.5$).
- (2) The characterization of range (B) for strong mixing, i.e., $\bar{F}(n, p')\geq 3$.
- (3) The characterization of a hierarchy of two time scales for the decay in range (A).
- (4) The prediction of a fast decay component in range (A), which manifests a residue of the np' doorway state.

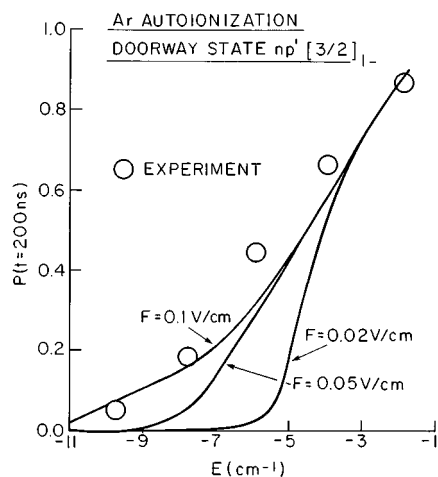


FIG. 10. Confrontation between the theoretical ZEKE spectra and the experimental results of Mühlpfordt and Even (Ref. 48) ($^2P_{1/2}np'[3/2]_1$ doorway state). The solid lines show the calculated ZEKE spectra for delay time $t=200$ ns at electric fields of $F=0.02, 0.05,$ and 0.1 V/cm (marked on the curves). The open points show the experimental data (Ref. 48).

- (5) The prediction of a distribution of very long lifetimes, with an average value of $\langle\tau_{\text{LONG}}\rangle$ in range (A). $\langle\tau_{\text{LONG}}\rangle$ (for a fixed n manifold) exceeds (by a numerical factor of 2–5) the strong mixing diluted value $\langle\tau(n)\rangle$, Eq. (4.10). $\langle\tau_{\text{LONG}}\rangle$ decreases with increasing n (at fixed F) and with increasing F (at fixed n) manifesting the enhancement of mixing.
- (6) The average lifetimes $\langle\tau(n)\rangle$ in range (B), which originate from a democratic dilution of all the doorway and escape states, can be well accounted for by a simple analytic result, Eq. (4.10).
- (7) In range (B), $\langle\tau(n)\rangle \propto n^4$, increasing fast with increasing n . The F dependence of $\langle\tau(n)\rangle$ (at fixed n) is very weak.

We shall confront our theoretical data for the ZEKE spectra and lifetimes (at fixed F) with the experimental results of Mühlpfordt and Even.⁴⁸ The main features for the theoretical ZEKE spectra (Fig. 10) are (i) The increase of the ZEKE signal ($P(t)$ at fixed t) with increasing n (or E) at fixed F , manifesting a transition from range (A) (at lower n) to range (B) (at high n). (ii) The appearance of low energy tails in range (A), which are more pronounced at higher F . (iii) For the relevant F values range (A) spans a rather broad n (and E) domain, which has to be handled by our complete treatment. (iv) The F independent increase of the spectrum for large n marks the attainment of range (B). The experimental spectral data (at the delay time $t=200$ and $F=0.1$ V/cm) reproduced in Fig. 10 from the work of Mühlpfordt and Even⁴⁸ exhibit a gradual increase, with an indication of a low energy tail. Reasonable agreement is found between our theoretical results and the experimental data for the ZEKE spectra⁴⁸ for $F=0.1-0.05$ V/cm (Fig. 10).

The main features of the theoretical lifetime data (Fig. 11) which are relevant for the analysis of the experimental data (at fixed F) are (i) In range (A) $\langle\tau_{\text{LONG}}(n)\rangle$ considerably exceeds (see point (5) above) the strong mixing value $\langle\tau_{\text{SM}}(n)\rangle$, Eq. (4.10). (ii) In range (A) $\langle\tau_{\text{LONG}}(n)\rangle$ decreases with increasing n . (iii) In range (B) $\langle\tau(n)\rangle$ increases with

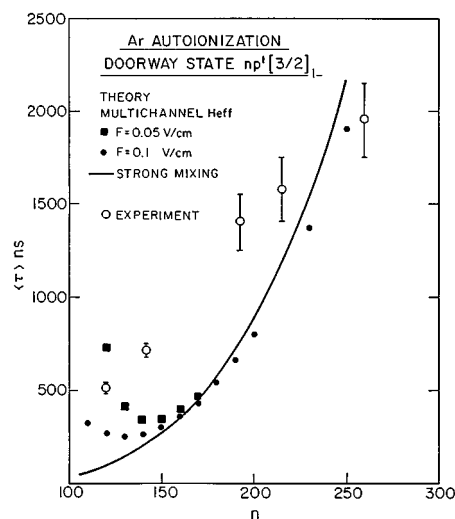


FIG. 11. The confrontation between the theoretical n dependence of the ZEKE lifetimes and the experimental lifetimes of Mühlpfordt and Even (Ref. 48) for Ar autoionization via the $^2P_{1/2}np'[3/2]_1$ doorway state. The solid line represents the strong mixing result $\langle\tau_{\text{SM}}(n)\rangle$, Eq. (4.10). (●) For $F=0.1$ V/cm and (■) for $F=0.05$ V/cm represent the calculated average lifetimes [for the decay of $P(t)$ in the range $t=200-1000$ ns] using the multichannel effective Hamiltonian. The open points (○) with error bars represent the experimental data (Ref. 48).

increasing n (i.e., $\propto n^4$). The experimental lifetime data $\tau(n)$,⁴⁸ at $n \leq 100$, are below experimental resolution. An abrupt increase of the experimental $\tau(n)$ at $n \approx 120$ to a large value of $\tau(120)=510$ ns is exhibited, followed by a gradual increase of $\tau(n)$ vs n in the range $n=120-260$.⁴⁸ These experimental data⁴⁸ are reproduced in Fig. 11. The experimental lifetimes⁴⁸ in the high n range, $n=190-260$, are compatible with our theoretical results for the strong mixing situation (Fig. 11). For the lower $n=120-150$ values a large positive deviation of the experimental $\tau(n)$ data⁴⁸ from the strong mixing results is exhibited (Fig. 11). These high values of $\tau(n)$ ($n=120-150$) are not inconsistent with the results of our analysis in range (A) for $F=0.05$ V/cm (Fig. 11).

Our analysis of the experimental results of Mühlpfordt and Even⁴⁸ provides the following conclusions. First, we identified the strong mixing regime where semiquantitative agreement between the experimental lifetime data and spectra and our theoretical predictions is obtained. Second, a tentative identification of range (A) in the ZEKE spectra and lifetimes for lower n ($n=150-120$) values was accomplished. These results provide partial information pertaining to predictions (1), (2), (5)–(7). For the time being, predictions (3) and (4) were not subjected to an experimental test, as they require short-time resolved (~ 10 ns) ZEKE spectroscopy, which has not yet been accomplished. From the theoretical point of view, our predictions, particularly those for range (A), require detailed experimental information on quantum defects $\delta(l)$, which are mostly available, and for the width parameters $\Gamma_0(IKJ)$, which are scarce. Even for the extensively studied Xe atom these parameters, well known for the ns' states,⁶⁴ are unknown for the np' states and are known within uncertainty of $\pm 30\%$ for the nd' states.⁶ Thus the theoretical hunting ground is, at present,

limited due to lack of input information for the construction of the effective Hamiltonian. Regarding our numerical procedure, we had diagonalized the effective Hamiltonian for a single n manifold. Two extensions are necessary. First, we have performed our calculations for the $M=0$ component of the ${}^2P_{1/2}n p'[3/2]_1$ triplet state. The inclusion of the $M=\pm 1$ components (with appropriate weights determined by experimental excitation conditions) should be performed. Second, this procedure, which disregards mixing between adjacent n manifolds, is valid, in principle, when $\bar{F} < 1/\delta(l')(\text{mod}1)$ for all the nl' doorway and escape states. We have shown,³⁸ on the basis of model calculations for a single doorway (and escape) state, that the effects of intermanifold mixing on the dynamics are small. Nevertheless, a detailed exploration of the dynamics of adjacent n manifolds will be of interest.

Our theoretical treatment provides a rather complete picture of the electric field induced dilution of the autoionization lifetimes. The dilution occurs for both the doorway state and the pure escape states within the ZEKE Rydberg manifold. The characteristics of the dilution are quantitatively different for $\langle\tau_{\text{LONG}}(n)\rangle$ in range (A) and for $\langle\tau\rangle=\langle\tau_{\text{SM}}(n)\rangle$ in range (B), as summarized by points (5) and (6). From the experimental point of view, one may attempt to adopt a simplified single channel analysis and consider a single escape state, which also constitutes the doorway state, i.e., the Ar $np'[3/2]_1$ state for the problem at hand. This approach is attractive to the experimentalist, as it involves the comparison between the lifetimes of lower n Rydbergs obtained from spectral line broadening and the lifetimes of ZEKE Rydbergs, as done by Merkt and by Mühlpfordt and Even for Ar^{31,48} and for large molecules.²⁸ This experimental dilution of the lifetime of a doorway (and escape) np' state in the strong mixing situation is $D(n)=\langle\tau_{\text{SM}}(n)\rangle/\tau(np')$, where $\langle\tau_{\text{SM}}(n)\rangle$ is given by Eq. (4.10) and $\tau(np')=n^3\hbar/\Gamma_0(p')$ with $\Gamma_0(p')=2100\text{ cm}^{-1}$.⁴⁸ The dilution factor is $D(n)=2n\Gamma_0(p')/\Gamma_0^T$, and making use of Eq. (4.9) we infer that

$$D(n)=2n\left[\Gamma_0(p')\left/\sum_{(lkJ)}\Gamma_0(lkJ)\right.\right]. \quad (5.1)$$

This dilution factor manifests the multichannel character of the dynamics, involving the decay widths of all the escape states. As the ratio

$$\rho=\left[\Gamma_0(p')\left/\sum_{(lkJ)}\Gamma_0(lkJ)\right.\right]\leq 1 \quad (5.2)$$

(being of the order of $\rho\sim 0.11$ for Ar autoionization via the np' doorway state), we expect that $D(n)=2n\rho\leq 2n$. This result constitutes a generalization of the general considerations advanced by Chupka,^{33,34} Bordas *et al.*,³⁵ and Merkt and Zare³⁶ who proposed that $D(n)=2n$. We have focused on atomic ionization, however, the universality principle for ZEKE Rydberg coupling and dynamics implies that Eq. (5.1) (with an appropriate extension of the definition of the widths parameters to include other nonradiative channels) is applicable for atoms, molecules and clusters, where one expects that $D(n)\propto n$ for the strong l mixing limit.³³⁻³⁵ As the ratio

of the widths parameters in Eq. (5.1) is expected to depend on the system, one expects that the system specificity of the dynamics will be manifested by the numerical proportionality factor in $D(n)$.

Searching for universal features of Rydberg ZEKE dynamics in atoms, molecules and clusters, we should focus on the strong mixing limit for which $\langle\tau_{\text{SM}}(n)\rangle=\xi\hbar n^4/\Gamma_0^T$ and $P_{\text{SM}}(t)\approx\exp(-t\Gamma_0^T/\xi\hbar n^4)$, where Γ_0^T is the sum of the widths parameters, and ξ a numerical constant (e.g., $\xi=2$ for the present problem). These simple results establish the universal features of a one-parameter (i.e., (Γ_0^T/ξ)) description of the dynamics in the strong mixing limit (B). This conclusion is borne out by our detailed numerical calculations. On the other hand, the elucidation of the Rydberg ZEKE dynamics in range (A) requires a full-fledged diagonalization of the effective Hamiltonian. In this range only general qualitative information, i.e., the hierarchy of two time scales, can be inferred without numerical analysis. For a quantitative description of the dynamics in range (A), a detailed analysis based on the multichannel effective Hamiltonian is required.

ACKNOWLEDGMENTS

We are grateful to Uzi Even for useful discussions, for extensive prepublication information and for his permission to quote his experimental results prior to publication. We are grateful to Frédéric Merkt for stimulating discussions, for communicating to us his unpublished ZEKE lifetime data and for his permission to quote his results prior to publication. We are grateful to Richard Bersohn, Ori Cheshnovsky, Raphael D. Levine, Edward W. Schlag, and Tim P. Softley for very useful discussions. This research was supported by the Binational German-Israel James Franck program for Laser-Matter Interaction.

APPENDIX A: SPECTROSCOPIC NOTATION

The Rydberg states of the heavier rare gas atoms (Ar, Kr, and Xe) are best characterized by the jl coupling scheme.⁶⁸⁻⁷⁰ j is the total angular momentum of the ionic core, l is the orbital angular momentum of the Rydberg electron, K is the resultant angular momentum from the coupling of j and l . K is weakly coupled to the electron spin s to give the total angular momentum of the atom J . The electronic states are labelled as ${}^2P_{jnl}[K]_J$. The two lowest electronic states of Ar⁺ are ${}^2P_{3/2}$ (first ionization potential IP1 = 127 110 ± 0.4 cm⁻¹) and ${}^2P_{1/2}$ (second ionization potential IP2 = 128 541.7 ± 0.3 cm⁻¹,⁷¹ and the more accurate value IP2 = 128 541.8 cm⁻¹.⁶³ The first Rydberg series converging to IP1 is ${}^2P_{3/2}nl[K]_J$. The autoionizing Rydberg series converging to IP2 is ${}^2P_{1/2}nl'[K]_J$, with the prime on l labelling $j=1/2$ states. In the autoionizing series ($j=1/2$) each value of l (except $l=0$) corresponds to four different states, i.e., $K=l\pm 1/2$ and $J=K\pm 1/2$.

APPENDIX B: AUTOIONIZATION DYNAMICS FOR THE RYDBERG MANIFOLDS EXCITED VIA THE ${}^2P_{1/2}nd'[3/2]_1$ DOORWAY STATE

We consider one-photon excitation of the Rydberg manifold from the ${}^1S_03p^6$ ground state, which was experimen-

tally studied by Merkt.³¹ The selection rules dictate excitation to the two series: ${}^2P_{1/2}ns'[1/2]_1$ and ${}^2P_{1/2}nd'[3/2]_1$. The asymptotic one-electron oscillator strengths⁴⁷ for hydrogenic orbitals for the $3p \rightarrow ns$ excitation is $0.3 n^{-3}$, while for the $3p \rightarrow nd$ excitation it is $6.1 n^{-3}$, with a ratio of oscillator strengths (at fixed n) being ~ 20 in favor of the

$3p \rightarrow nd$ excitations. Thus the overwhelming transition probability is to the ${}^2P_{1/2}nd'[3/2]_1$ series. For each n manifold the ${}^2P_{1/2}nd'[3/2]_1$ state constitutes the doorway state. The doorway singlet state ${}^2P_{1/2}nd'[3/2]_1$ ($M=0$) interacts according to the selection rules (4.1) with six escape states. The multichannel effective Hamiltonian for this problem is

$s'[1/2]_1$	\exists	\exists	0	0	0	0	
\exists	$p'[1/2]_0$	0	\exists	0	0	0	
\exists	0	$p'[3/2]_2$	\exists	\exists	0	0	
0	\exists	\exists	$d'[3/2]_1$	0	\exists	0	\dots
0	0	\exists	0	$d'[5/2]_3$	\exists	\exists	
0	0	0	\exists	\exists	$f'[5/2]_2$	0	
0	0	0	0	\exists	0	$f'[7/2]_4$	
			\vdots				\ddots

(B1)

The Stark couplings (denoted by \exists) between l and $l+1$ (for $\Delta S = \Delta M = \Delta j = 0$) are given by Eqs. (4.2) and (4.3) and have the following forms:

For $K = l - 1/2$, $J = l - 1$ $\{\Delta K = \Delta J = \Delta l = 1\}$:

$$\langle J, K, l | z | J+1, K+1, l+1 \rangle = \frac{[l(l+1)]^{1/2}}{2l+1} \langle \nu l | r | \nu' l+1 \rangle, \quad (\text{B2})$$

for $K = l + 1/2$, $J = l + 1$ $\{\Delta K = 0, \Delta J = \Delta l = 1\}$:

$$\langle J, K, l | z | J-1, K, l+1 \rangle = \frac{1}{2(l+1)^2(2l+3)} \langle \nu l | r | \nu' l+1 \rangle, \quad (\text{B3})$$

and for $K = l + 1/2$, $J = l + 1$ $\{\Delta K = \Delta J = \Delta l = 1\}$:

$$\langle J, K, l | z | J+1, K+1, l+1 \rangle = \frac{[(l+1)(l+2)]^{1/2}}{2l+3} \langle \nu l | r | \nu' l+1 \rangle. \quad (\text{B4})$$

The onsets of effective mixing, Eq. (4.4) and for strong mixing, Eq. (4.6), are lower for the nd' states than for the np' series (Fig. 2). Typical $\bar{F}(n, d')$ data are summarized in Table II. In the limit of strong mixing ($\bar{F}(n, d') > 3$) the average lifetime of a ZEKE n manifold accessible via the nd' doorway state is given by $\langle \tau_{\text{SM}}(n) \rangle = 2n^4 \hbar / \Gamma_0^T$, Eq. (4.10), with $\Gamma_0^T = 40\,800 \text{ cm}^{-1}$ as obtained from Eq. (4.9) and the data of Table I for the effective Hamiltonian (B1). The limiting decay times are summarized in Table II. Numerical calculations performed by the diagonalization of the effective Hamiltonian for n values which correspond to range (A) (for a fixed value of F) resulted in the increase of the long time (low-amplitude) component $\langle \tau_{\text{LONG}}(n) \rangle$ by a numerical factor of 2–5 relative to the limiting values of Table II, in analogy with the results for the np' doorway state (Sec. V).

Merkt's time-resolved ZEKE spectroscopy^{31,72} (at low background field $F \approx 0.1 \text{ V/cm}$) for the Ar autoionizing Rydberg manifolds excited via the ${}^2P_{1/2}nd'[3/2]_1$ doorway state, exhibits the following features:

- An onset of the ZEKE spectrum (at the decay time $t_D = 200 \text{ ns}$) is exhibited at $n \approx 70-75$.^{31,72} This onset corresponds to average lifetimes⁷² $\langle \tau \rangle \approx 30-50 \text{ ns}$ for $n \approx 75-78$.
- A gradual increase of the amplitude of the ZEKE spectrum ($t_D = 200 \text{ ns}$)^{31,72} and of the lifetimes⁷² towards higher n values is exhibited. For $n \approx 91$ the average lifetime is $\langle \tau \rangle \approx 250 \text{ ns}$.⁷²
- A broad peak in the ZEKE spectrum ($t_D = 200 \text{ ns}$) occurs at $\nu \approx 120-180$.^{31,72}
- A sharp drop of the ZEKE spectrum at $n > 180$ is exhibited. The amplitude of the ZEKE spectrum drops to zero at $\Delta E = 3.2 \text{ cm}^{-1}$ below $\text{IP} = 128\,541.8 \text{ cm}^{-1}$,⁷² i.e., at $n = 185$. This energy shift is somewhat higher than expected for the field-induced shift of the ionization potential, i.e., $\Delta E(\text{calculated}) = 1.9 \text{ cm}^{-1}$ ($n = 240$) for $F = 0.1 \text{ V/cm}$.

We can now confront Merkt's experimental results^{31,72} with our calculations. The experimental onset of long lifetimes at $n = 70-75$ [observation (a)] is in agreement with our theory. According to the $\bar{F}(n, d')$ data of Table II, the region $n = 70-80$ corresponds to the onset of effective mixing under Merkt's experimental conditions^{31,72} ($F = 0.1 \text{ V/cm}$), with $\bar{F}(n, d') = 0.3-0.6$, corresponding to the onset of range (A). For n values just above the onset of range (A) we expect that the (average) long lifetime is

$$\langle \tau_{\text{LONG}}(n) \rangle = \eta(n) \langle \tau_{\text{SM}}(n) \rangle, \quad (\text{B5})$$

with the parameters $\eta(n) \approx 3-5$. From Table II we then infer that $\langle \tau_{\text{LONG}}(70) \rangle \approx 20-30 \text{ ns}$ and $\langle \tau_{\text{LONG}}(80) \rangle \approx 30-60 \text{ ns}$, in reasonable agreement with experimental data⁷² near the threshold of range (A). This analysis does also provide a

proper rationalization for the observation^{31,48,72} that the onset of effective nd doorway state mixing ($n \approx 70-80$ at $F \approx 0.1$ V/cm) is exhibited at lower values of n than for the np' doorway state mixing ($n \approx 100$ at $F = 0.1$ V/cm). However, for the dynamics of autoionization via the ${}^2P_{1/2}nd'[3/2]_1$ state,^{31,73} the agreement between theory and experiment ends here. Range (A) for effective mixing, according to Eqs. (4.4) and (4.6), is realized (for $F = 0.1$ V/cm) in the range $n = 80-110$ (Table II). In range (A) we expect $\langle \tau_{\text{LONG}}(n) \rangle$ to decrease with increasing n . This prediction is in contrast with the experimental lifetime data^{31,72} where the experimental $\langle \tau(n) \rangle$ increases with increasing n [point (b)] in the range $n = 75-91$.^{31,72} Furthermore, the experimental lifetimes for higher n Rydbergs in range (A) (point (b) above) are considerably longer than predicted on the basis of Eq. (B5) with $\eta(n) \rightarrow 1$ for $n \rightarrow 110$. For example, for $n = 91$ we expect (Table II) $\langle \tau_{\text{LONG}}(90) \rangle \approx 50-90$ ns, which is considerably lower than the experimental estimate⁷² $\langle \tau(91) \rangle \approx 250$ ns. This considerably longer experimental lifetime than that predicted on the basis of our theory for l mixing, may be due to lm_l mixing, originating from ion-Rydberg collisions, as suggested by Merkt³¹ and by Merkt and Zare.³⁶

Another interesting effect pertains to the electric field reduction of $P(t)$ (fixed t), which is substantial for $F = 1-2$ V/cm.³¹ Our analysis for l mixing predicts a much smaller effect at considerably lower values of F ($\approx 0.01-0.1$ V/cm). Our conclusions, which consider the dynamics of a single n manifold, are inconsistent with the quantitative features of Merkt's results.³¹ It was suggested by Merkt and Zare^{31,36} that this electric field effect is due to (lm_l) mixing between adjacent n manifolds. We have shown³⁸ that for a single doorway (and escape) state the effects of intermanifold (l) mixing is small. A further theoretical exploration of the multichannel problem with several adjacent n manifolds will be undertaken. Of course, further experimental progress, in conjunction with further theoretical explorations, e.g., collisional effects proposed by Chupka,^{33,34} (lm_l) mixing induced by the electric field of ions already proposed by Merkt and Zare,³⁶ and (lm_l) mixing induced by magnetic field effects, will be of considerable interest.

¹J. Liang, M. Gross, P. Goy, and S. Haroche, Phys. Rev. A **33**, 4437 (1986).

²*Long Range Casimir Forces*, edited by F. S. Levin and D. A. Micha (Plenum Press, New York, 1993).

³J. Müller and J. Burgdörfer, Phys. Rev. Lett. **70**, 2375 (1993).

⁴M. L. Zimmerman, M. G. Littman, M. M. Kash, and D. Kleppner, Phys. Rev. A **20**, 2251 (1979).

⁵R. D. Knight and L. Wang, Phys. Rev. A **32**, 896 (1985).

⁶L. Wang and R. D. Knight, Phys. Rev. A **34**, 3902 (1986).

⁷P. Brevet, M. Pellarin, and J. L. Vialle, Phys. Rev. A **42**, 1460 (1990).

⁸W. E. Ernst, T. P. Softley, and R. N. Zare, Phys. Rev. A **37**, 4172 (1988).

⁹H. H. Fielding and T. P. Softley, J. Phys. B **25**, 4125 (1992).

¹⁰*Rydberg States of Atoms and Molecules*, edited by R. F. Stebbins and F. B. Dunning (Cambridge University, Cambridge, 1983).

¹¹J. Wang and R. E. Olson, Phys. Rev. Lett. **72**, 332 (1994).

¹²(a) H. Beutler, Z. Phys. **86**, 710 (1933); (b) U. Fano, Nuovo Cimento **12**, 156 (1935).

¹³U. Fano, Phys. Rev. **124**, 1866 (1961).

¹⁴H. Lefebvre-Brion and R. W. Field, *Perturbations in the Spectra of Diatomic Molecules* (Academic, Orlando, 1986).

¹⁵E. Miescher, Can. J. Phys. **54**, 2074 (1976).

¹⁶A. Glusti-Suzor and Ch. Jungen, J. Chem. Phys. **80**, 986 (1984).

¹⁷J. Jortner, J. Chim. Phys. Special Issue, *Transitions non Radiatives Dans Les Molécules*, p. 9 (1969).

¹⁸J. Jortner and S. Leach, J. Chim. Phys. **77**, 7 (1980); **77**, 43 (1980).

¹⁹J. Jortner and G. C. Morris, J. Chem. Phys. **51**, 3689 (1969).

²⁰R. L. Whetten, S. G. Grubb, C. E. Otis, A. C. Albrecht, and E. R. Grant, J. Chem. Phys. **82**, 1115 (1985).

²¹A. Amirav and J. Jortner, J. Chem. Phys. **82**, 4378 (1985).

²²K. Müller-Dethlefs, M. Sander, and E. W. Schlag, Chem. Phys. Lett. **112**, 291 (1984).

²³K. Müller-Dethlefs, M. Sander, and E. W. Schlag, Z. Naturforsch. Teil A **38**, 1089 (1984).

²⁴G. Reiser, W. Habenicht, K. Müller-Dethlefs, and E. W. Schlag, Chem. Phys. Lett. **152**, 119 (1988).

²⁵K. Müller-Dethlefs and E. W. Schlag, Ann. Rev. Phys. Chem. **42**, 109 (1991).

²⁶(a) W. G. Scherzer, H. L. Selzler, E. W. Schlag, and R. D. Levine, Phys. Rev. Lett. **72**, 1435 (1994). (b) W. G. Scherzer, H. L. Selzler, and E. W. Schlag, Z. Naturforsch. Teil A **48**, 1256 (1993).

²⁷X. Zhang, J. M. Smith, and J. L. Knee, J. Chem. Phys. **99**, 3133 (1993).

²⁸U. Even, R. D. Levine, and R. Bersohn, J. Phys. Chem. **98**, 3472 (1994).

²⁹D. Bahatt, U. Even, and R. D. Levine, J. Chem. Phys. **98**, 1744 (1993).

³⁰U. Even, M. Ben-Nun, and R. D. Levine, Chem. Phys. Lett. **210**, 416 (1993).

³¹F. Merkt, J. Chem. Phys. **100**, 2623 (1994).

³²E. Rabani, L. Ya. Baranov, R. D. Levine, and U. Even, Chem. Phys. Lett. **221**, 473 (1994).

³³W. A. Chupka, J. Chem. Phys. **98**, 4520 (1993).

³⁴W. A. Chupka, J. Chem. Phys. **99**, 5800 (1993).

³⁵C. Bordas, P. F. Brevet, M. Broyer, J. Chevalere, P. Labastie, and J. P. Perrot, Phys. Rev. Lett. **60**, 917 (1988).

³⁶F. Merkt and R. N. Zare, J. Chem. Phys. **101**, 3495 (1994).

³⁷J. Jortner and M. Bixon, J. Chem. Phys. **102**, 5636 (1995).

³⁸M. Bixon and J. Jortner, J. Phys. Chem. **99**, 7466 (1995).

³⁹M. Bixon and J. Jortner (to be published).

⁴⁰R. S. Berry, J. Chem. Phys. **45**, 1228 (1966).

⁴¹N. Bradzley, Chem. Phys. Lett. **1**, 229 (1967).

⁴²A. Russek, M. R. Patterson, and R. L. Becker, Phys. Rev. **167**, 167 (1967).

⁴³G. Herzberg and C. Jungen, J. Mol. Spectrosc. **41**, 425 (1992).

⁴⁴C. Jungen and D. Dill, J. Chem. Phys. **73**, 3338 (1980).

⁴⁵R. S. Mulliken, J. Am. Chem. Soc. **91**, 4615 (1969).

⁴⁶M. Rault and C. Jungen, J. Chem. Phys. **74**, 3388 (1981).

⁴⁷H. A. Bethe and E. E. Salpeter, *Quantum Mechanics of One- and Two-Electron Atoms* (Springer-Verlag, Berlin, 1957).

⁴⁸A. Mühlfordt and U. Even, J. Chem. Phys. **103**, 4427 (1995).

⁴⁹(a) D. A. Harmin, Phys. Rev. A **24**, 2491 (1981); (b) **26**, 2656 (1982); (c) **30**, 2413 (1984); (d) K. Sakimoto, J. Phys. B **19**, 3011 (1986); (e) **22**, 2727 (1989).

⁵⁰(a) M. Bixon and J. Jortner, J. Chem. Phys. **48**, 715 (1968); (b) Mol. Cryst. **213**, 237 (1969).

⁵¹M. Bixon and J. Jortner, Isr. J. Chem. **1**, 189 (1969).

⁵²M. Bixon and J. Jortner, J. Chem. Phys. **50**, 3284 (1969).

⁵³M. Bixon and J. Jortner, J. Chem. Phys. **50**, 4061 (1969).

⁵⁴M. Bixon, Y. Dothan, and J. Jortner, Mol. Phys. **17**, 109 (1969).

⁵⁵S. Mukamel and J. Jortner, in *The World of Quantum Chemistry*, edited by R. Daudel and B. Pullman (Reidel Publ. Co., 1974), p. 109.

⁵⁶S. Mukamel and J. Jortner, in *MTP International Review of Science*, edited by A. D. Buckingham and C. A. Coulson (Butterworth, London, 1976), Vol. 13, p. 327.

⁵⁷S. Mukamel and J. Jortner, in *Excited States*, edited by E. C. Lim (Academic, New York, 1977), Vol. III, pp. 57-107.

⁵⁸(a) U. Fano, Phys. Rev. A **2**, 353 (1970); (b) U. Fano, J. Opt. Soc. Am. **65**, 979 (1975).

⁵⁹F. Merkt (private communication).

⁶⁰(a) K. Radler and J. Berkowitz, J. Chem. Phys. **70**, 216 (1979); (b) K. Radler and J. Berkowitz, *ibid.* **70**, 221 (1979).

⁶¹J. Berkowitz, Advances Chem. Phys. **58**, 1 (1988).

⁶²J. Z. Wu, S. B. Whitfield, C. Caldwell, M. O. Krause, P. M. Meulen, and A. Fahlman, Phys. Rev. A **42**, 1350 (1990).

⁶³K. Yoshino, J. Opt. Soc. Am. **60**, 1220 (1970).

⁶⁴D. Klar, K. Harth, J. Ganz, T. Kraft, M. W. Ruf, H. Hotop, V. Tsemekhman, K. Tsemekhman, and M. Ya. Amusia, Z. Phys. D **23**, 101 (1992).

⁶⁵A. R. Edmonds, J. Picart, N. T. Minh, and R. Pullen, J. Phys. B **12**, 2781 (1979).

⁶⁶J. S. Howard, J. P. Riola, R. D. Rundel, and R. F. Stebbins, Phys. Rev. Lett. **29**, 321 (1972).

⁶⁷R. F. Stebbings and F. B. Dunning, Phys. Rev. A **8**, 665 (1973).

⁶⁸G. Racah, Phys. Rev. **61**, 537 (1942).

⁶⁹R. D. Rundel, F. B. Dunning, H. C. Goldwire, and R. F. Stebbings, J. Opt. Soc. Am. **65**, 628 (1975).

⁷⁰M. Amyar, O. Robaux, and C. Thomas, J. Phys. B **14**, 4255 (1981).

⁷¹C. E. Moore, *Atomic Energy Levels*, Natl. Bur. Stand. U.S. Circular No. 467 (U.S. GPO, Washington, D.C., 1958), Vol. 1.

⁷²F. Merkt (private communication) (to be published).